A Panoramic Photograph of the Galactic Bar from Long period Variables

Han-Yuan Zhang

Collaborators: Vasily Belokurov, N. Wyn Evans, Sarah G. Kane, Jason L. Sanders

Structures at the inner Galaxy

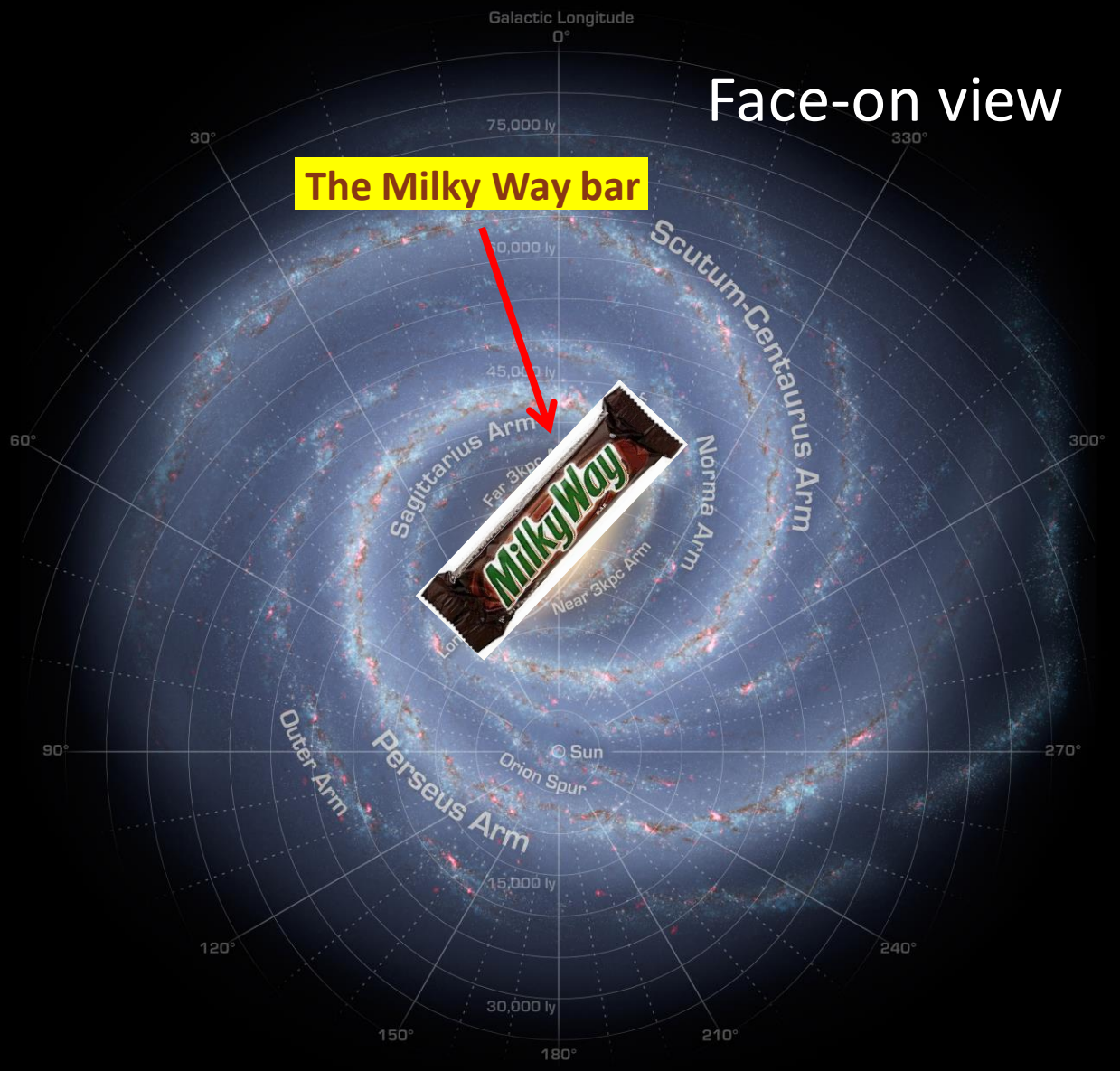

Structures at the inner Galaxy

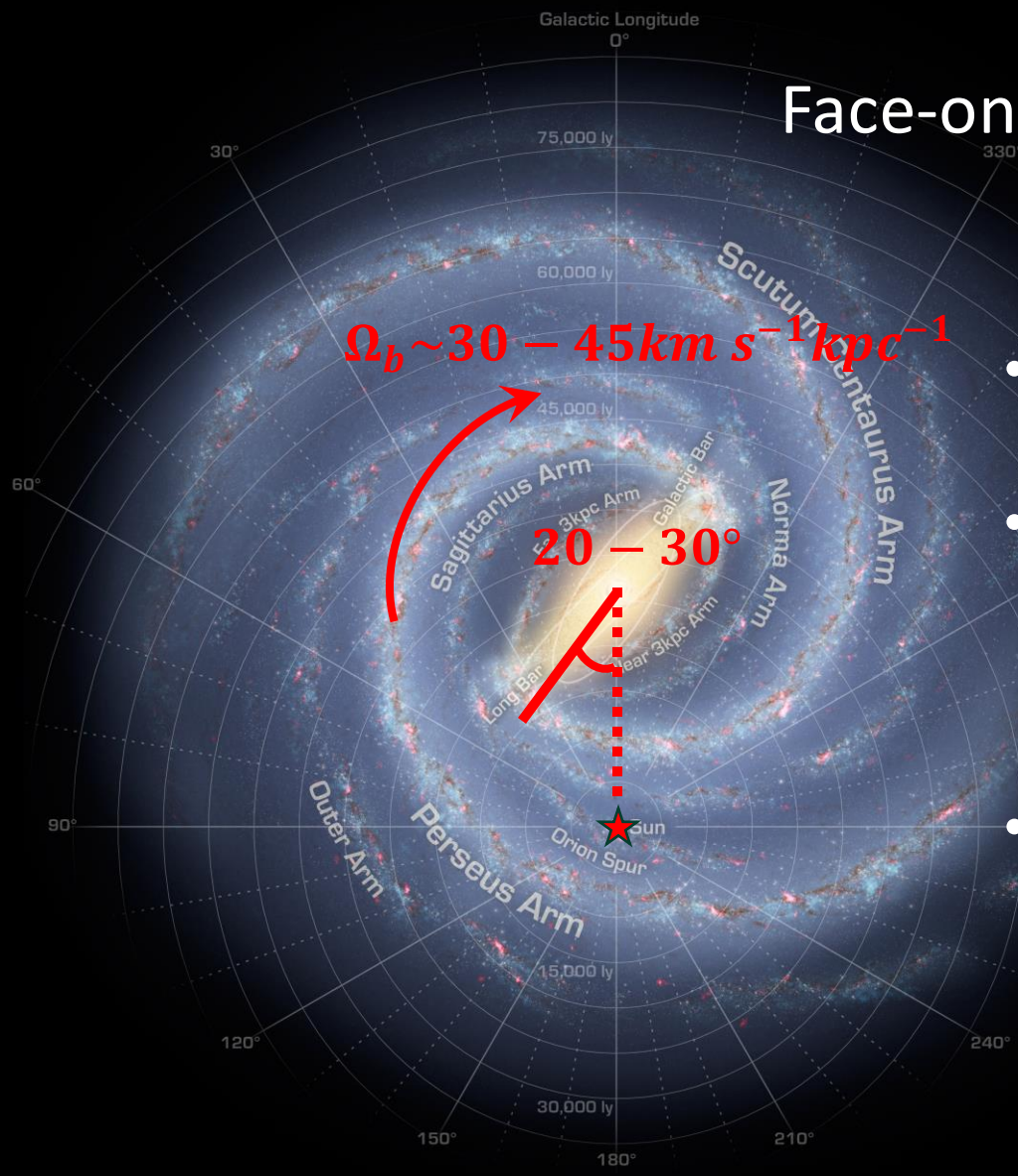

- Dynamics at the inner Galaxy
- Kinematic and equilibrium in the solar neighbourhood, disc, and halo
- Star formation history

Previous “photographs” of the Galactic bar:

Bovy+19, Queiroz+21 using spectroscopic distances

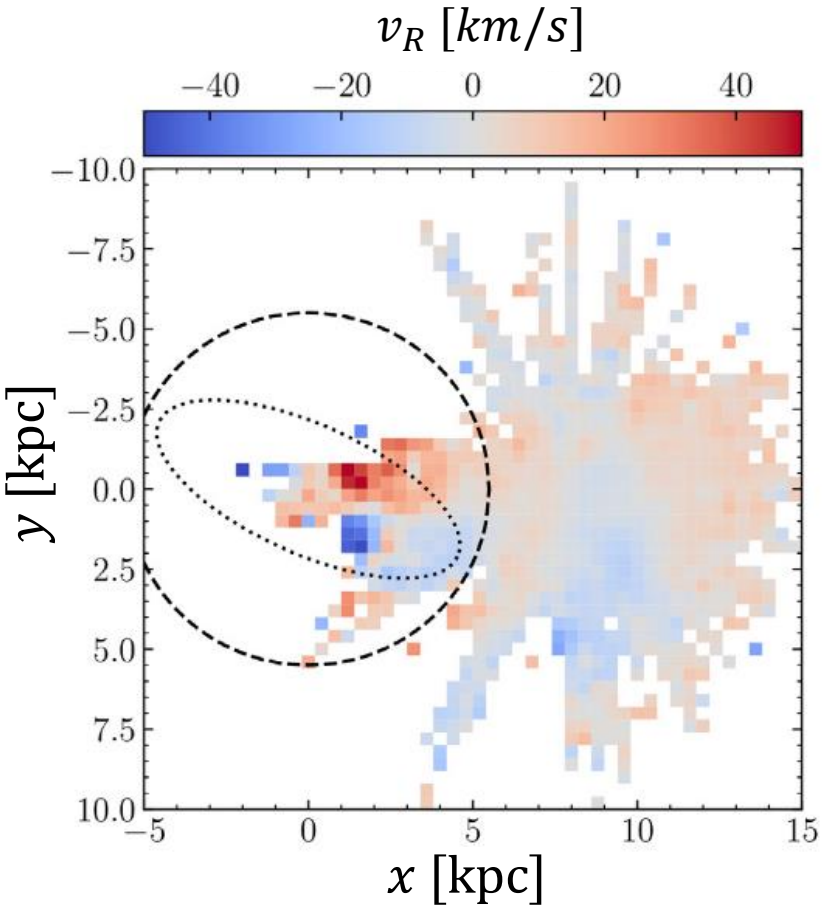

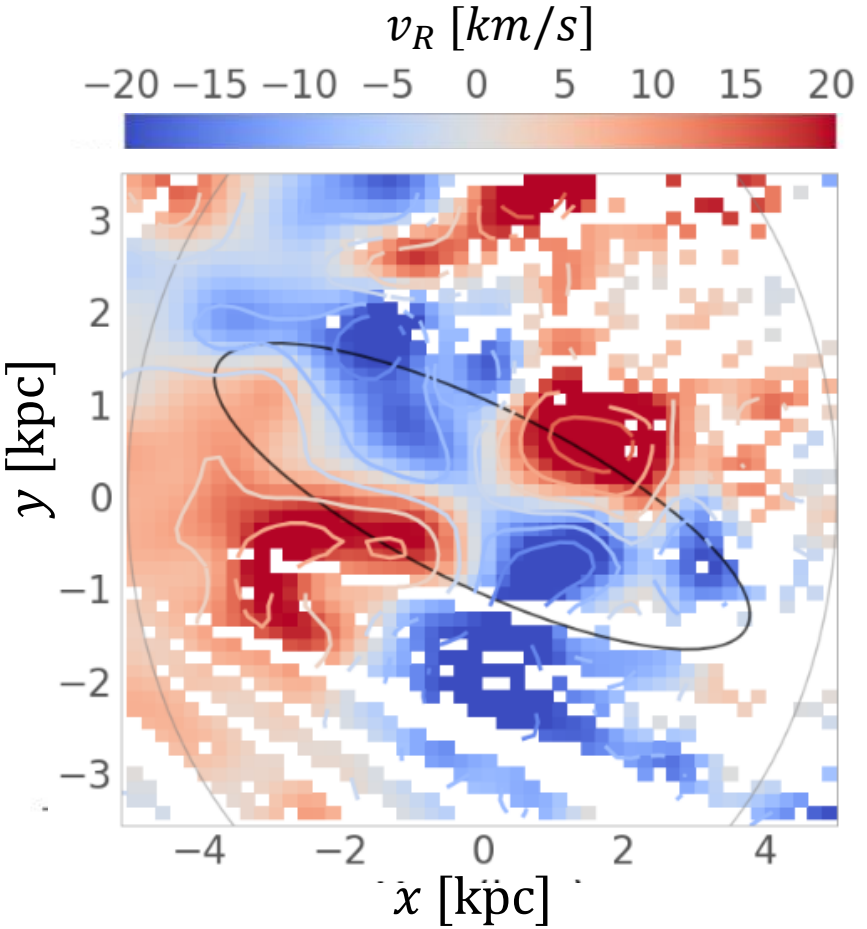

Bovy+19: APOGEE-AstroNN distances

Also see Leung+23 for an updated version

Queiroz+21 : APOGEE-StarHorse distances

Previous “photographs” of the Galactic bar:

Hey+23 using semi-regular variables in the OGLE survey

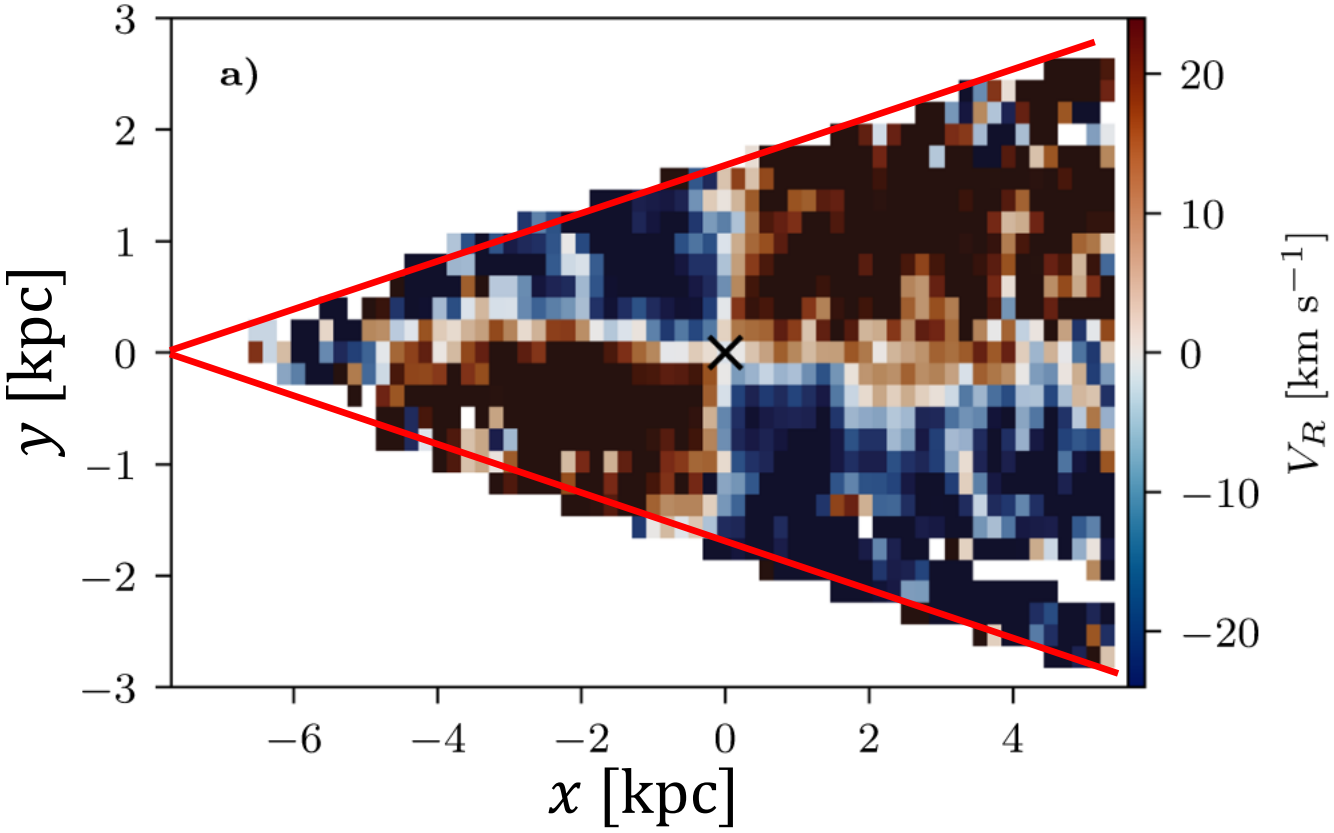

Hey+23

Low-amplitude Long-period Variables (LA-LPV)

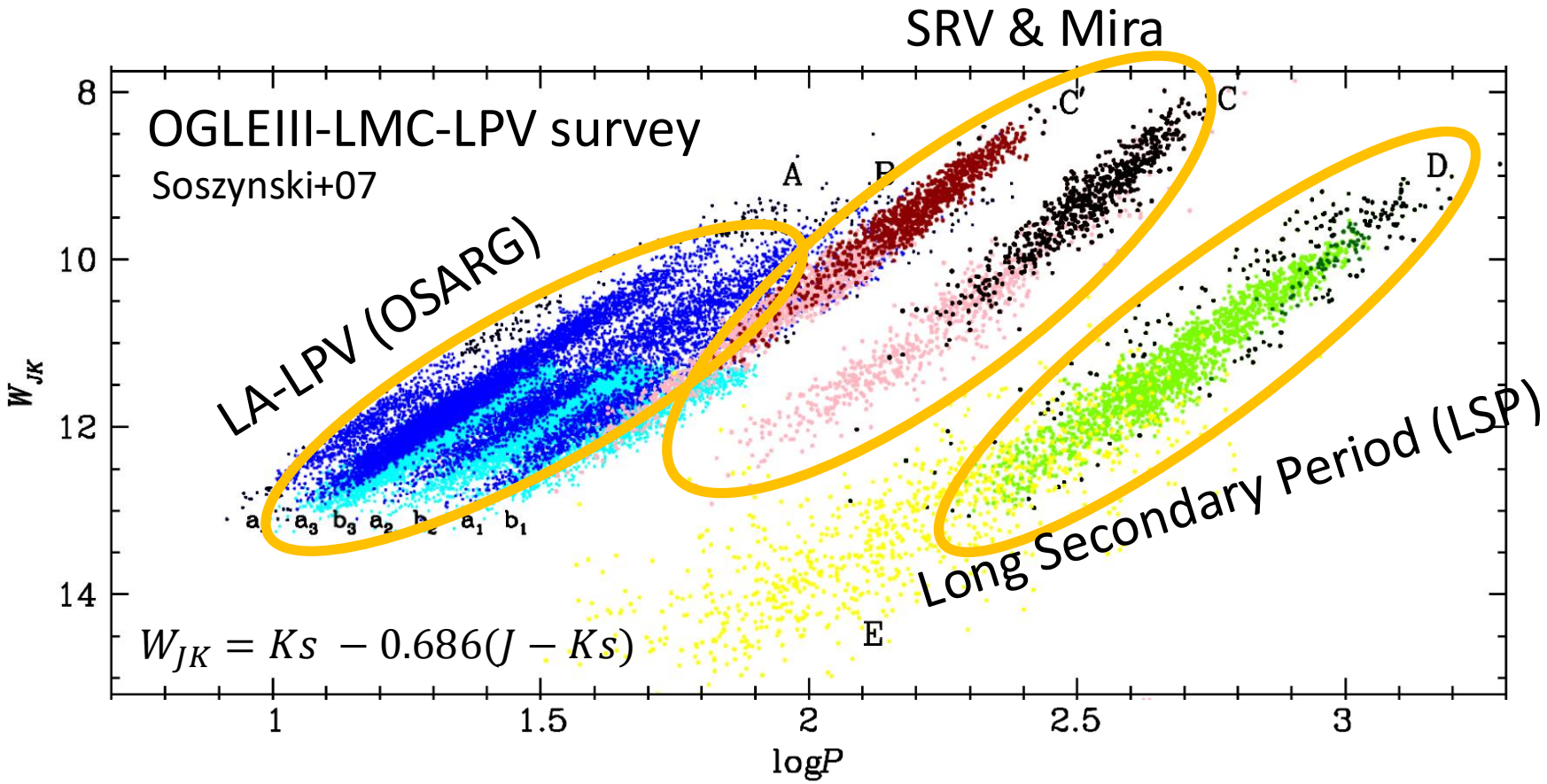

LA-LPVs follows tight period-luminosity relation and hence are good indicators with distance uncertainty 10-15%
(Rau+19, Hey+23 & HZ+ in prep).

Period-Luminosity plane in Gaia LPV catalogue

- We can isolate LA-LPV (OSARG) candidates from the Gaia LPV catalogue by cutting on the amplitude and period

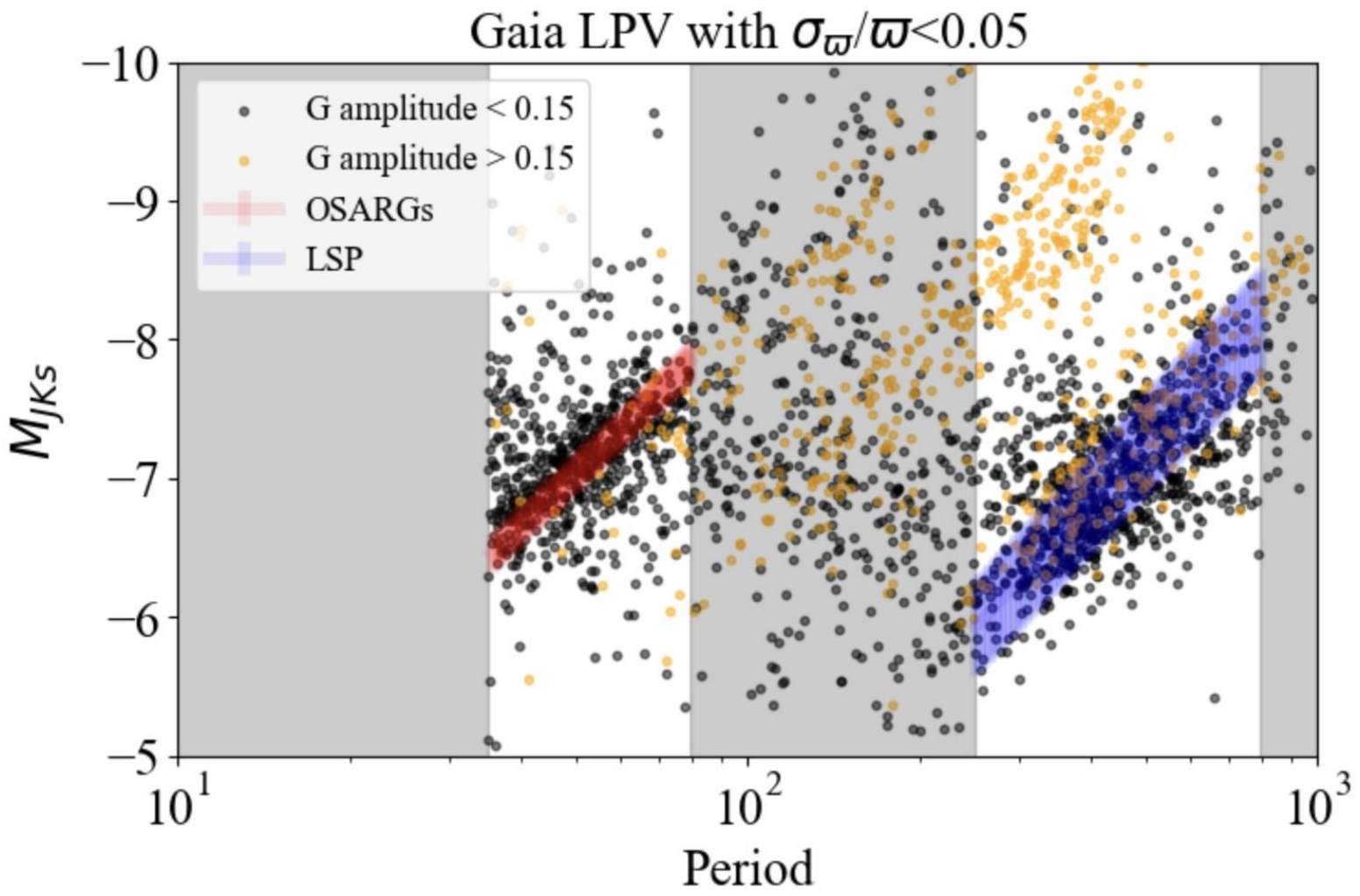

Spatial distribution of LA-LPV in this sample

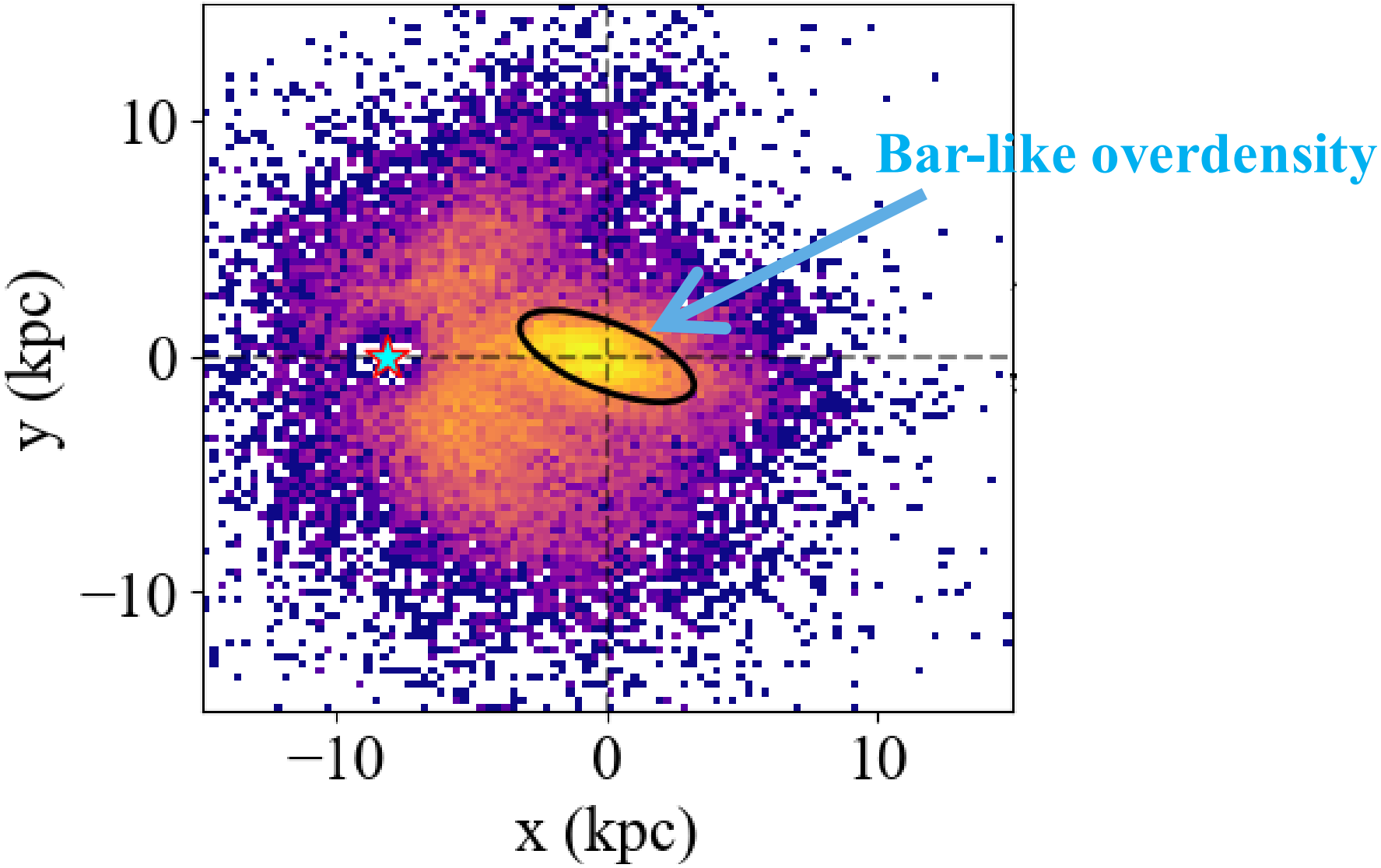

~34000 stars with full 6D phase space measurements & ~20000 are in the inner 5 kpc

Kinematics of the LA-LPV sample

Bar signature: Quadrupole v_R pattern

- Quadrupole pattern seen due to the streaming motion of the bar
- Sign-switching line biased towards the Sun-GC (Galactic centre) line due to the distance uncertainty
  (see Hey+23; Vislosky+24; Liao+24)

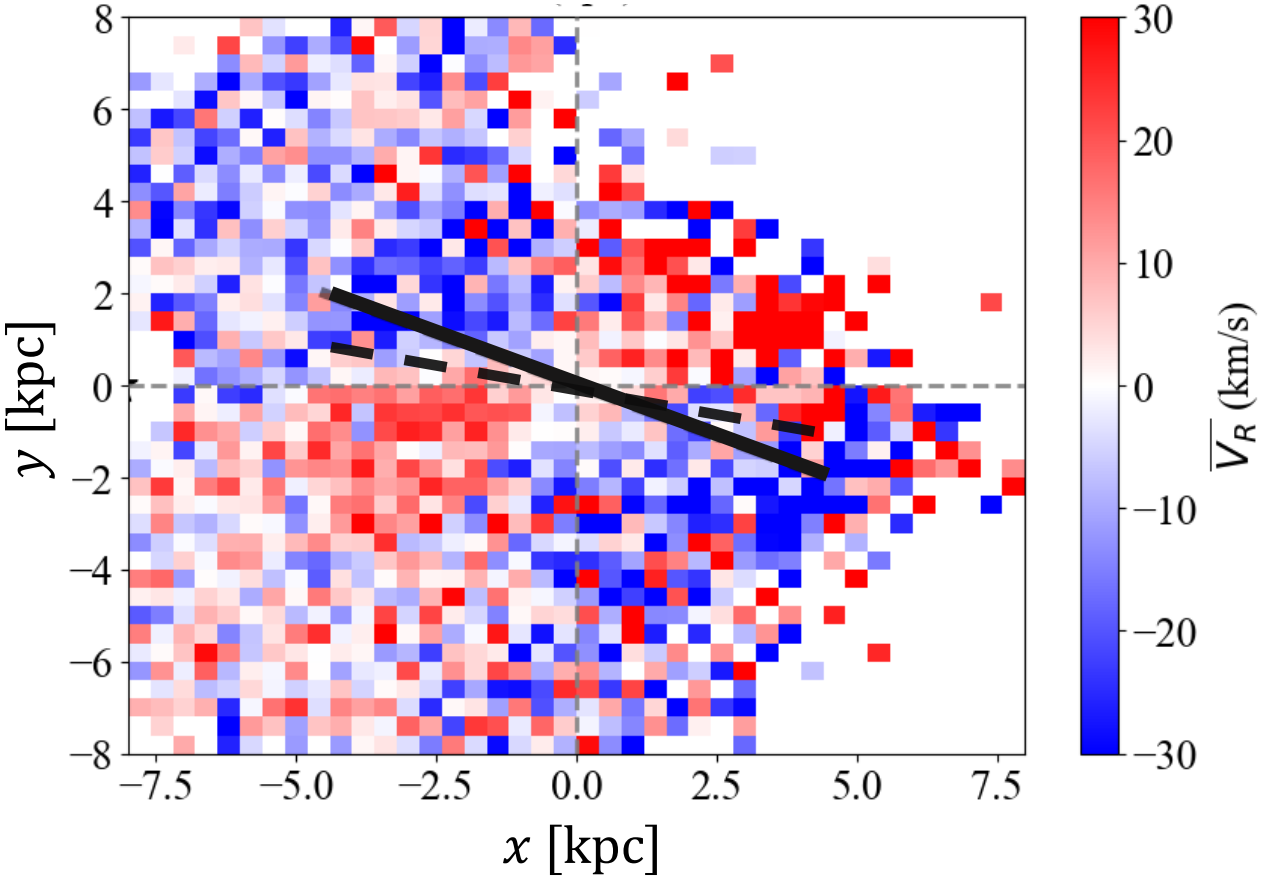

Kinematics of the LA-LPV sample

$$\left\langle \left| \frac{v_R}{v_{\rm tot}} \right| \right\rangle = \frac{1}{N} \sum_j^N \frac{|v_{R,j}|}{v_{{\rm tot},j}},$$

Bar signature: $\langle |v_R|/v_{tot} \rangle$ *map*

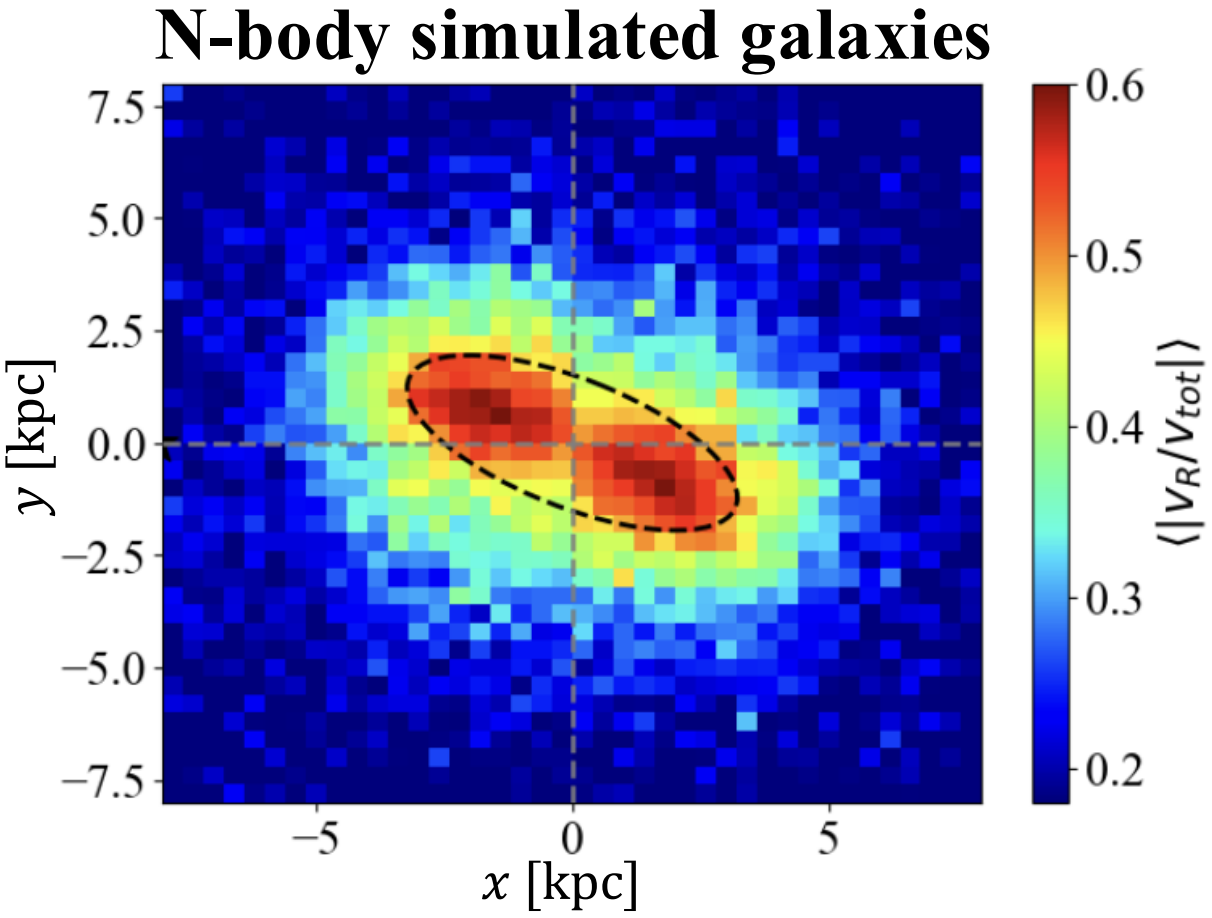

Kinematics of the LA-LPV sample

$$\left\langle \left| \frac{v_R}{v_{\rm tot}} \right| \right\rangle = \frac{1}{N} \sum_j^N \frac{|v_{R,j}|}{v_{{\rm tot},j}},$$

Bar signature: $\langle |v_R|/v_{tot} \rangle$ *map*

- High value is expected in the bar region due to the orbital structures of bar-supporting stars
- Less affected by the distance uncertainty as $\langle |v_R|/v_{tot} \rangle$ is a dimensionless quantity

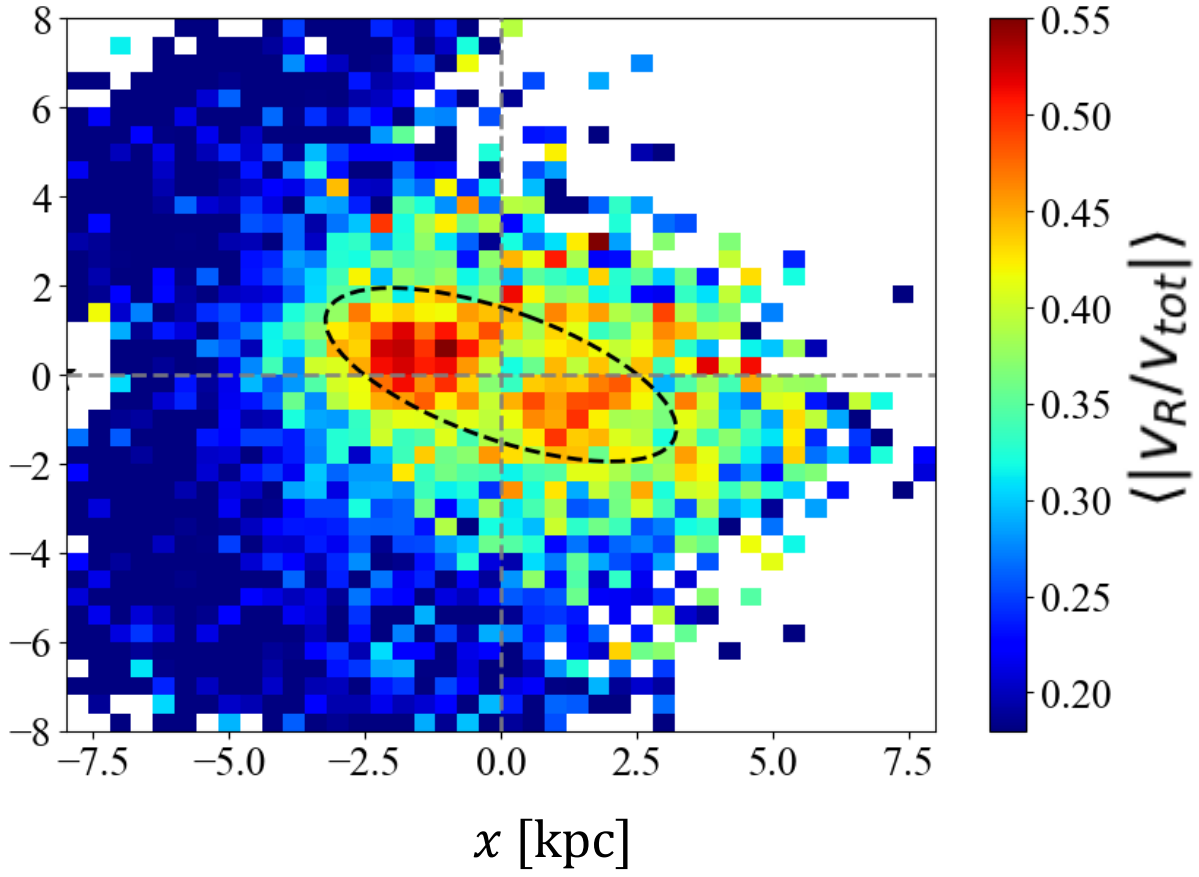

Bar length measurement

- Traditionally measured from the stellar overdensity, but the existence of a connected spiral arm would leading to an overestimated bar length (see Hilmi+20)

- Dynamical length, defined as the radius spanned by the bar-supporting orbits, would be less affected by the connected spiral arm

- Motivation: measure the dynamical length model-independently using purely kinematics

Mock Galaxy A

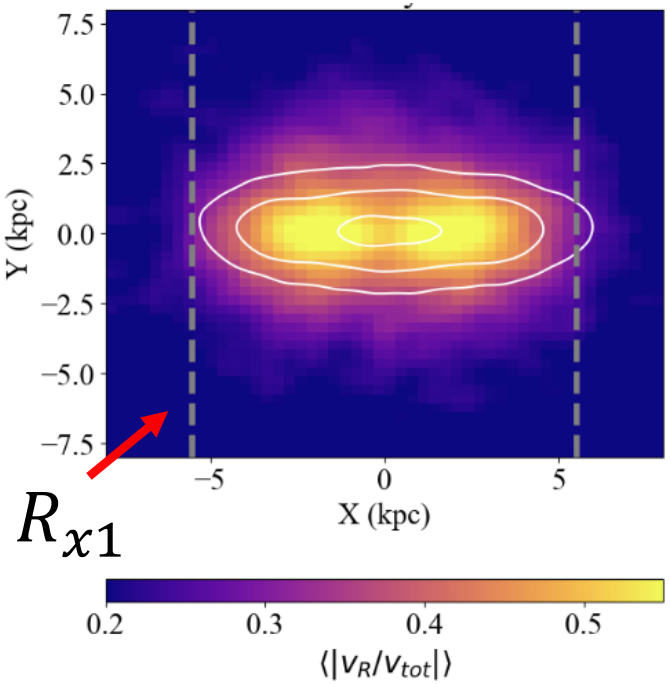

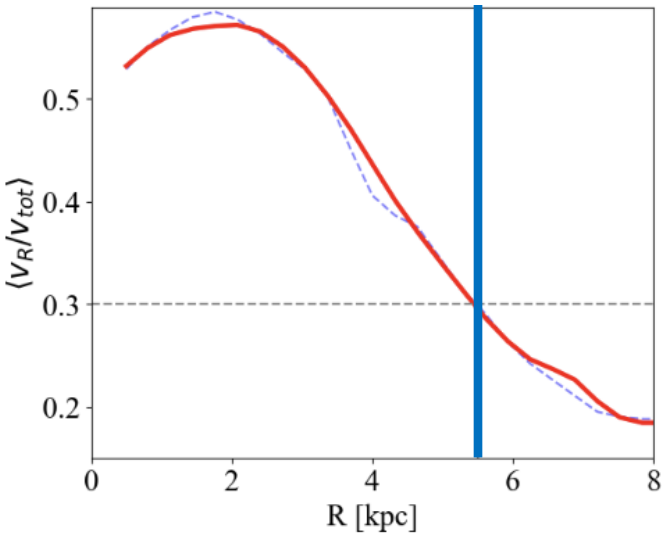

Mock Galaxy B

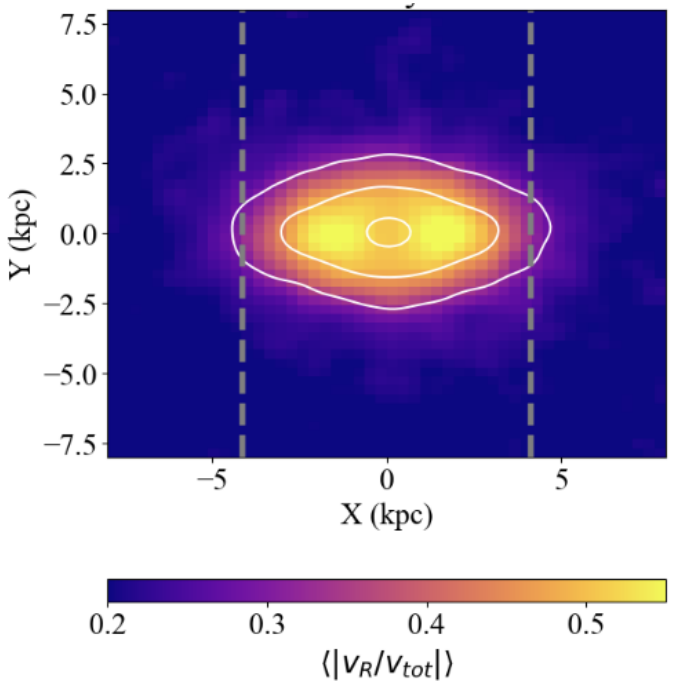

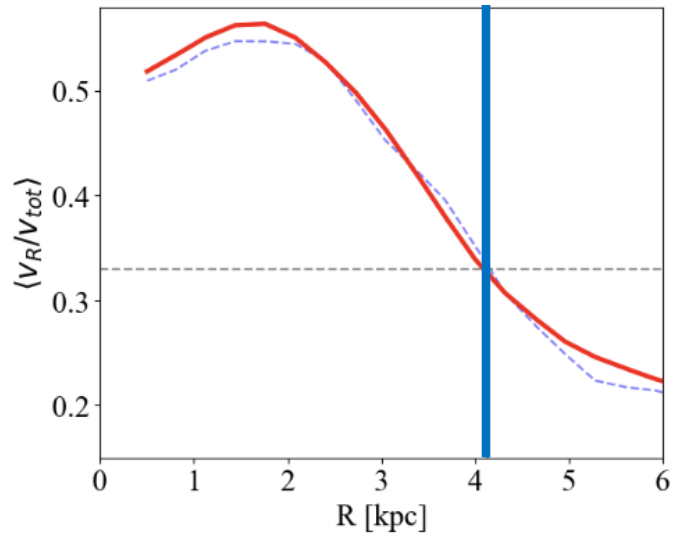

LA-LPV sample

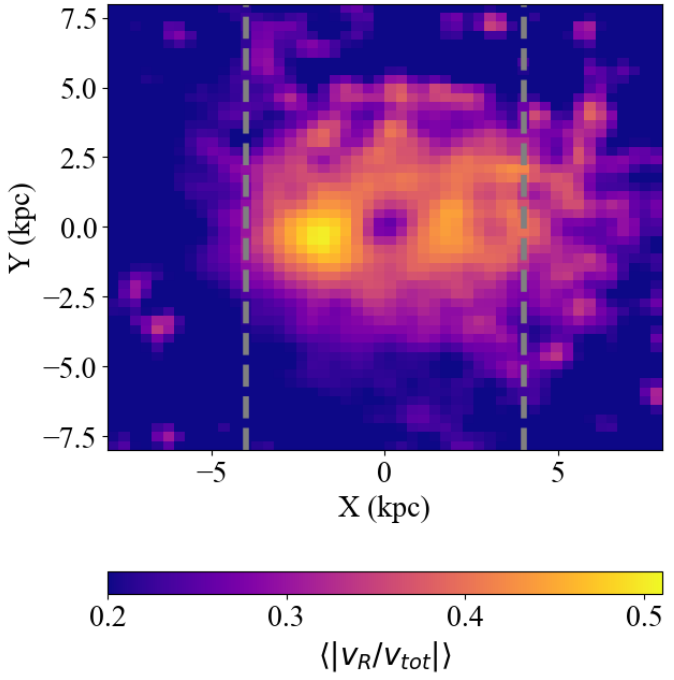

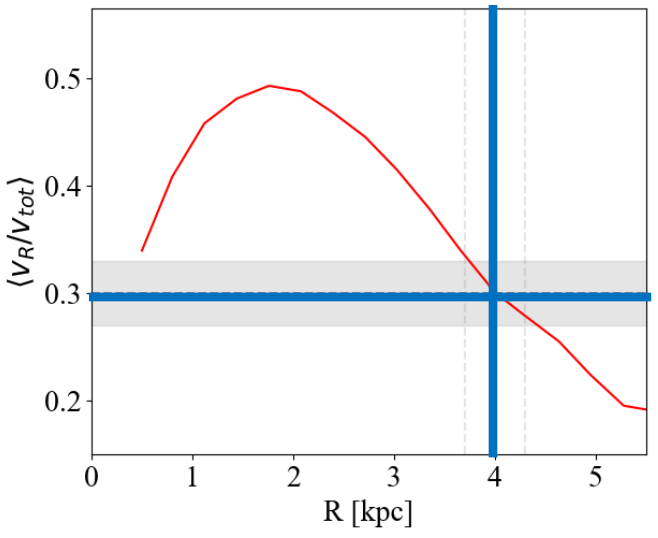

Estimation of the pattern speed

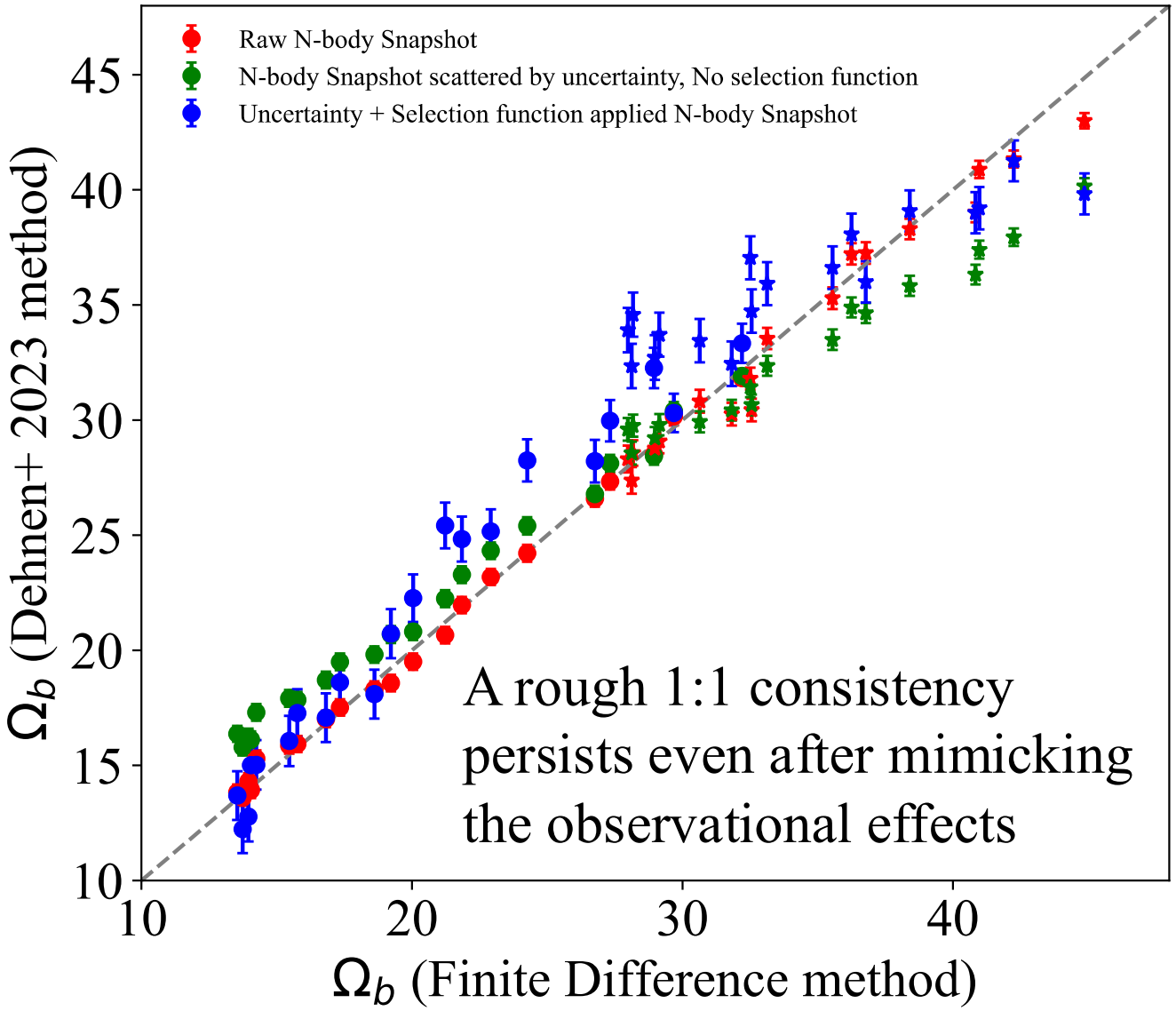

$$\partial\rho/\partial t + \nabla\cdot(\rho\bar{\boldsymbol{v}}) = 0$$

Dehnen+23

$$\Omega = \frac{\int \mathrm{d}^3\boldsymbol{x}\ \rho\left[W\bar{\dot{\varphi}} + \frac{\mathrm{i}}{m}\bar{v}_R(\partial W/\partial R)\right]\mathrm{e}^{-\mathrm{i}m\varphi}}{\int \mathrm{d}^3\boldsymbol{x}\ \rho\, W\,\mathrm{e}^{-\mathrm{i}m\varphi}}.$$

Apply the method in Dehnen+23 to the LA-LPV sample yields

$$\boldsymbol{\Omega_b \sim 34.1 \pm 2.4\ km\ s^{-1} kpc^{-1}}$$

for the Milky Way bar

Consistent to other observations using different methods (see Dillamore+23,24; Clarke&Gerhard 22, etc.)

Orbital families in the Galactic bar

- Assume the Galactic potential from the M2M model in Portail+17 (Sormani+22) is correct
- Select bar stars with $1.8 < \Omega_R/\Omega_X < 2.2$
- Shed light on the vertical structure of the bar using the Ω_Z/Ω_X value

Ω = Orbital frequencies

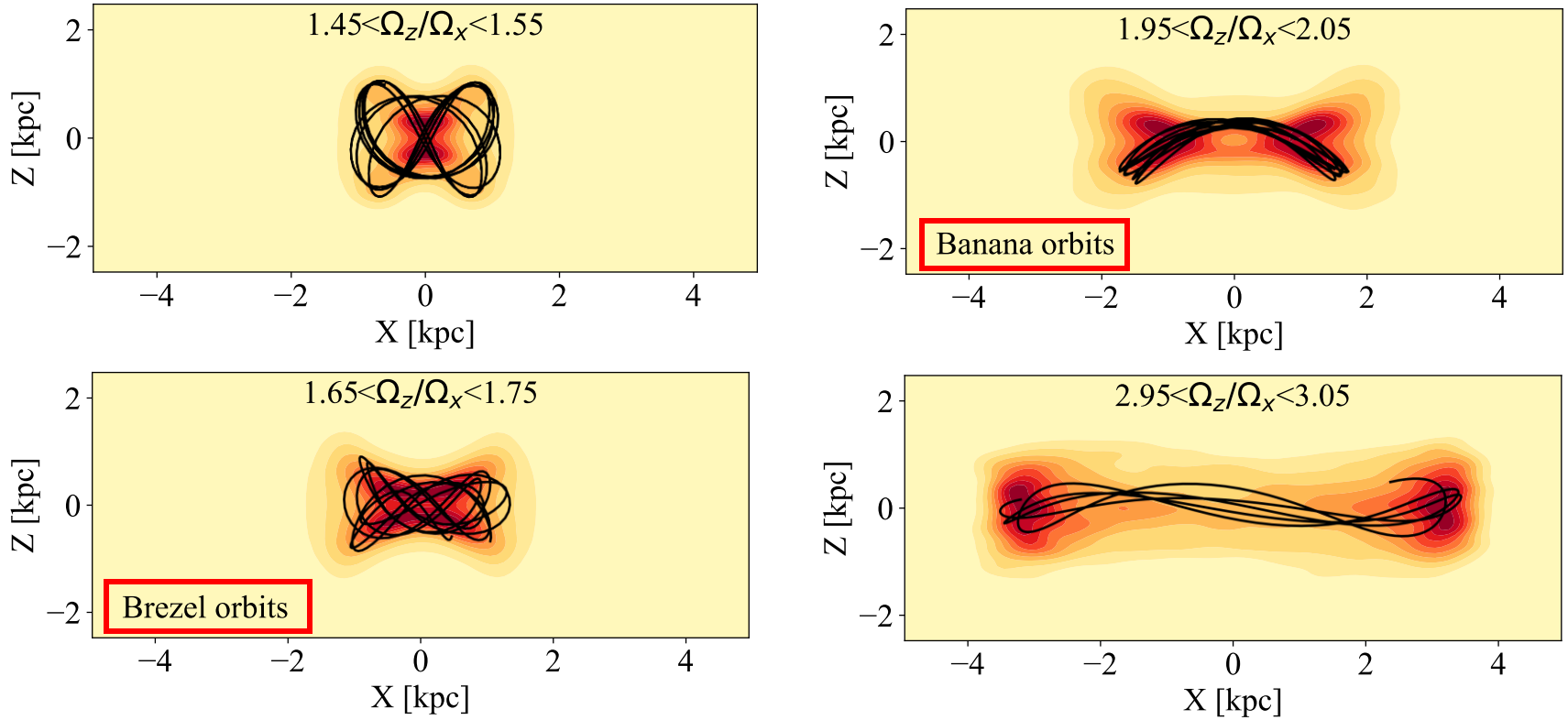

What contribute the Galactic X-shaped stucture

Banana or Brezel ?

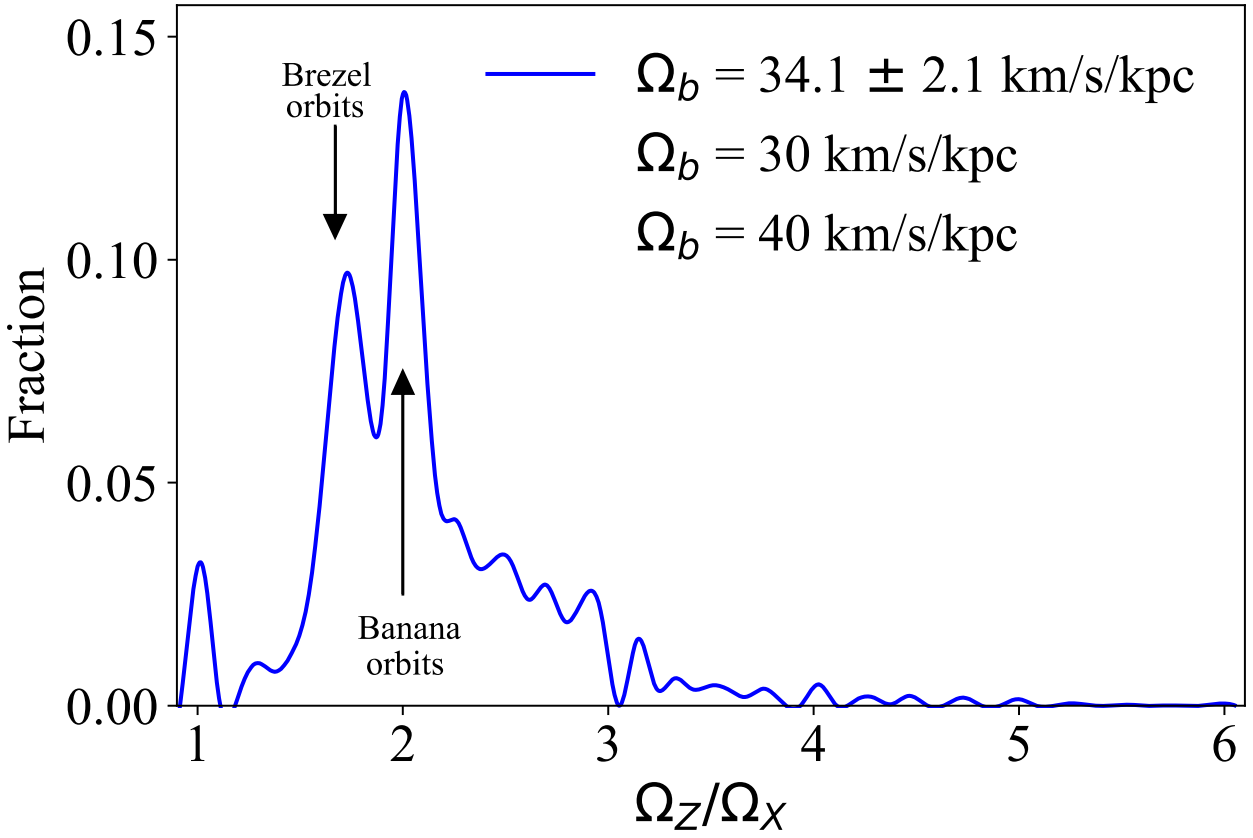

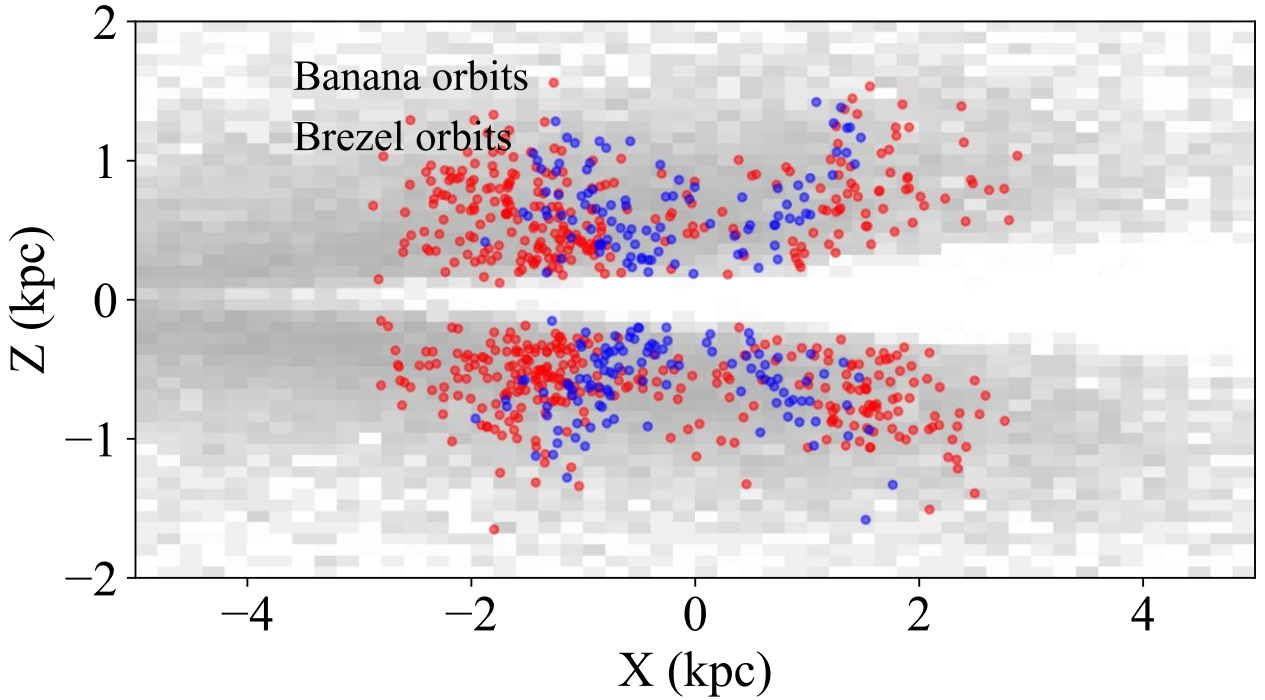

Summary

- We use LA-LPV as unbiased tracers to take a “panoramic photograph” of the inner Galaxy in full 6D phase space
- We constrain the kinematics field of the inner Galaxy:
  - Quadrupole pattern in v_R maps
  - Bisymmetric pattern in $\langle v_R/v_{tot} \rangle$ map
- We use the continuity equation to calculate the pattern speed of the bar $\Omega_{\rm b} \sim 34.1 \pm 2.4$ km s^{-1}kpc^{-1}
- We demonstrate that the radial $\langle v_R/v_{tot} \rangle$ profile can model-independently yield a kinematic analogue of the dynamical length of the bar $R_{\rm b,\,kine} \sim 4.0$ kpc
- We study the orbital families in the Galactic bar and show that the banana orbits are still the main constituent of the Galactic X-shaped structure, although the contribution from other orbital families cannot be ignored

arxiv:2406.06678

Previous “photographs” of the Galactic bar:

Wegg+15 using red clump stars

Wegg+15

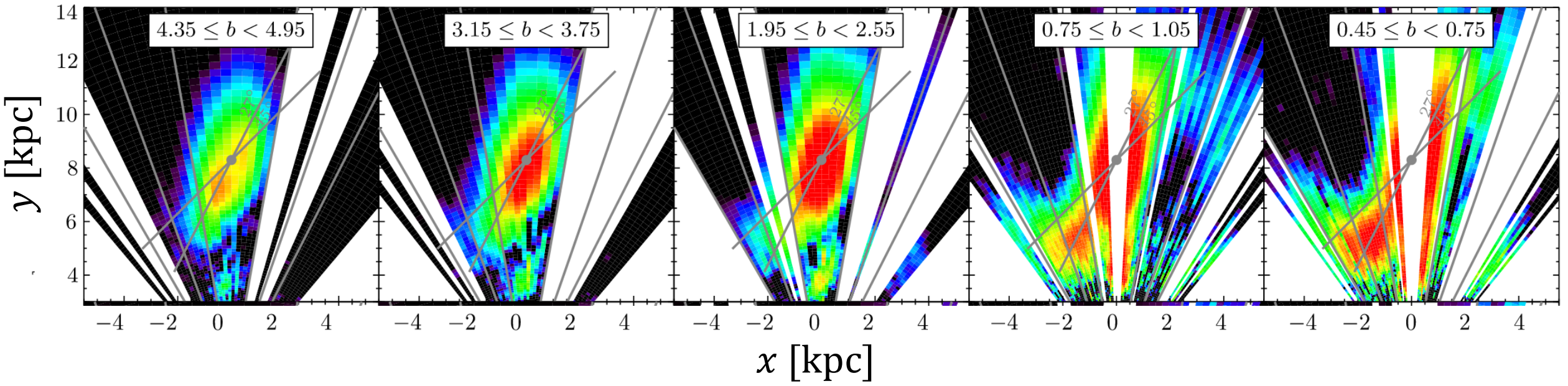

Problem: Don’t resolve individual stars & no full phase space

Low-amplitude, Long-period variable (LA-LPV)

- It is also called OGLE Small Amplitude Red Giants (OSARG)
- Long-period: $P \sim 10 - 100\ day$
- Low-amplitude: $\Delta G \sim ?\ - 0.2\ mag$
- Multi-periodic behaviour: light curves are composed by multiple characteristic period; also, it has multiple period-luminosity sequences
- Unbiased tracers: does not favours old or young population like RR-lyrae or Cepheids

The accuracy and precision of the luminosity distances

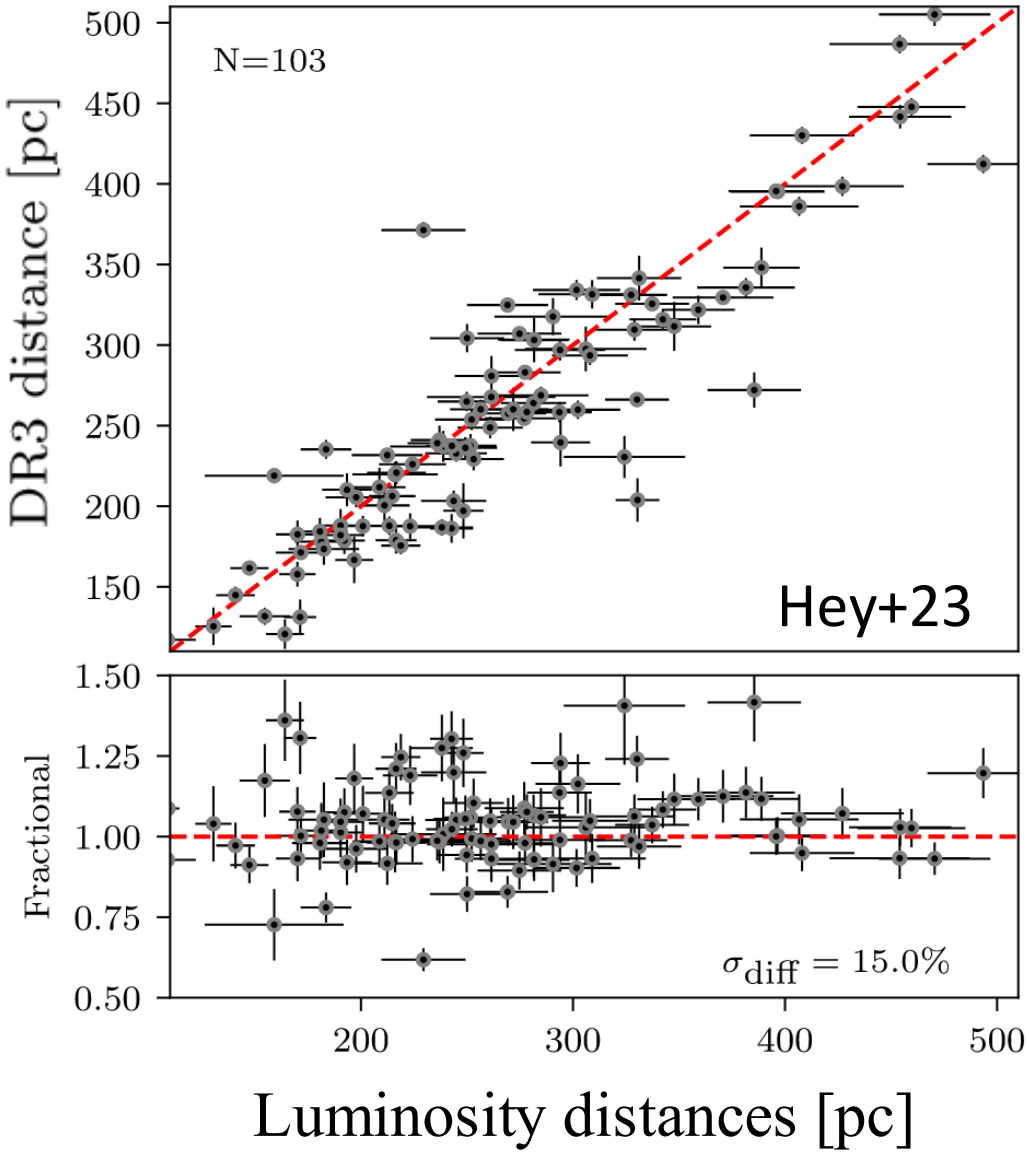

Zhang et.al in prep.

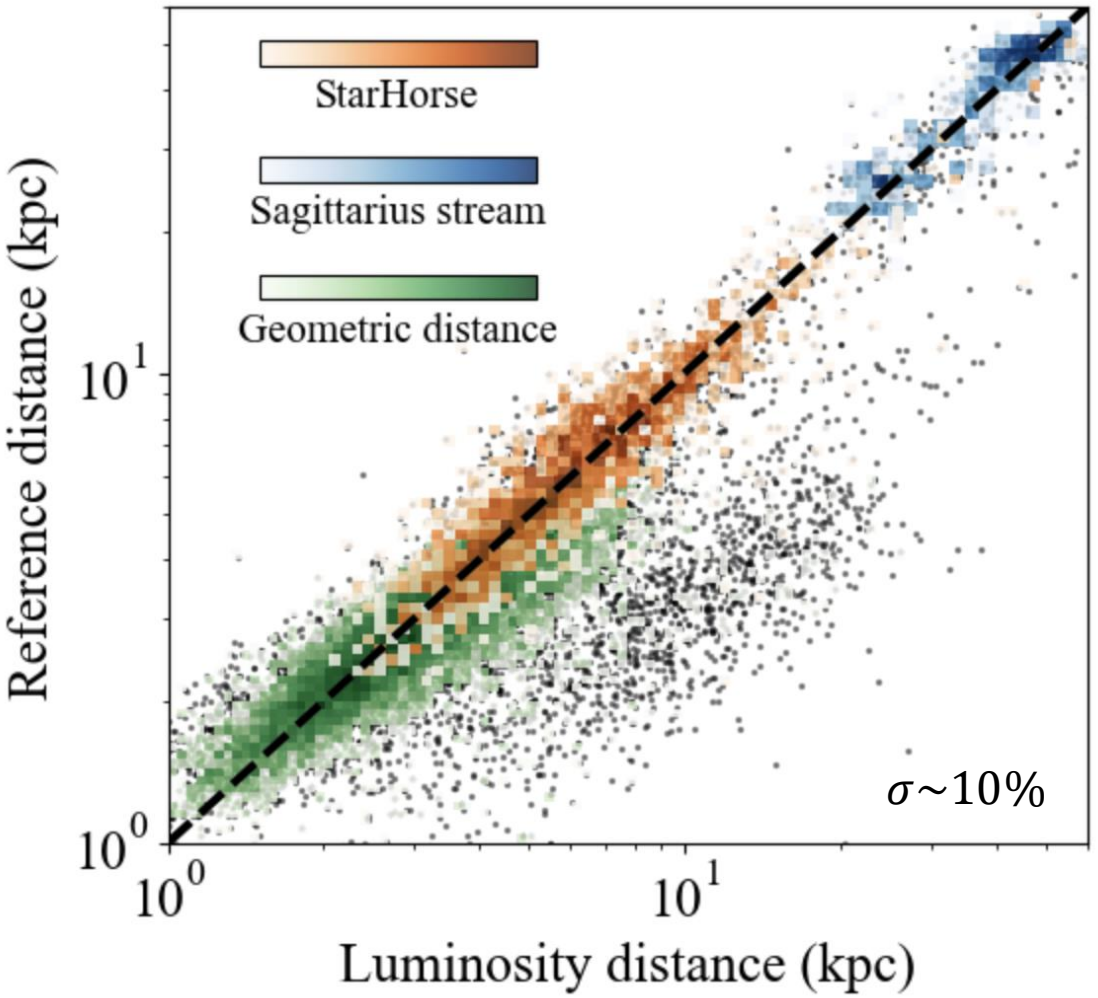

Validation of luminosity distances

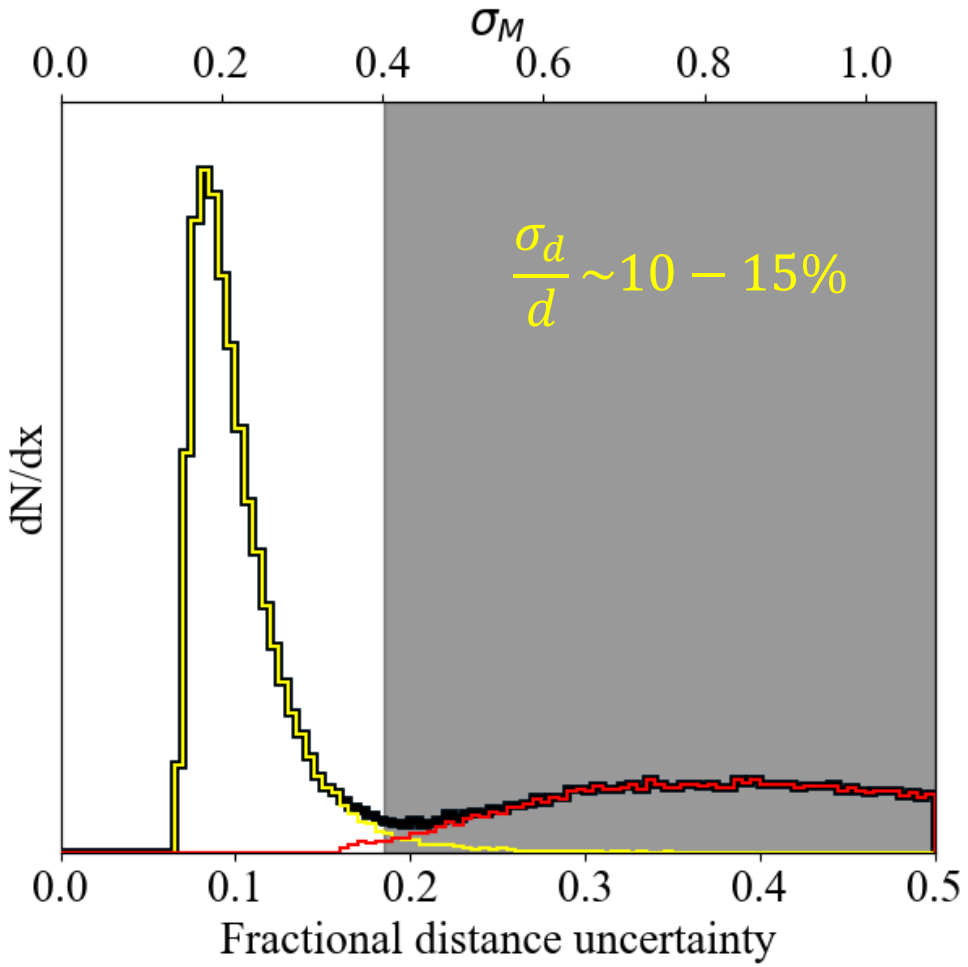

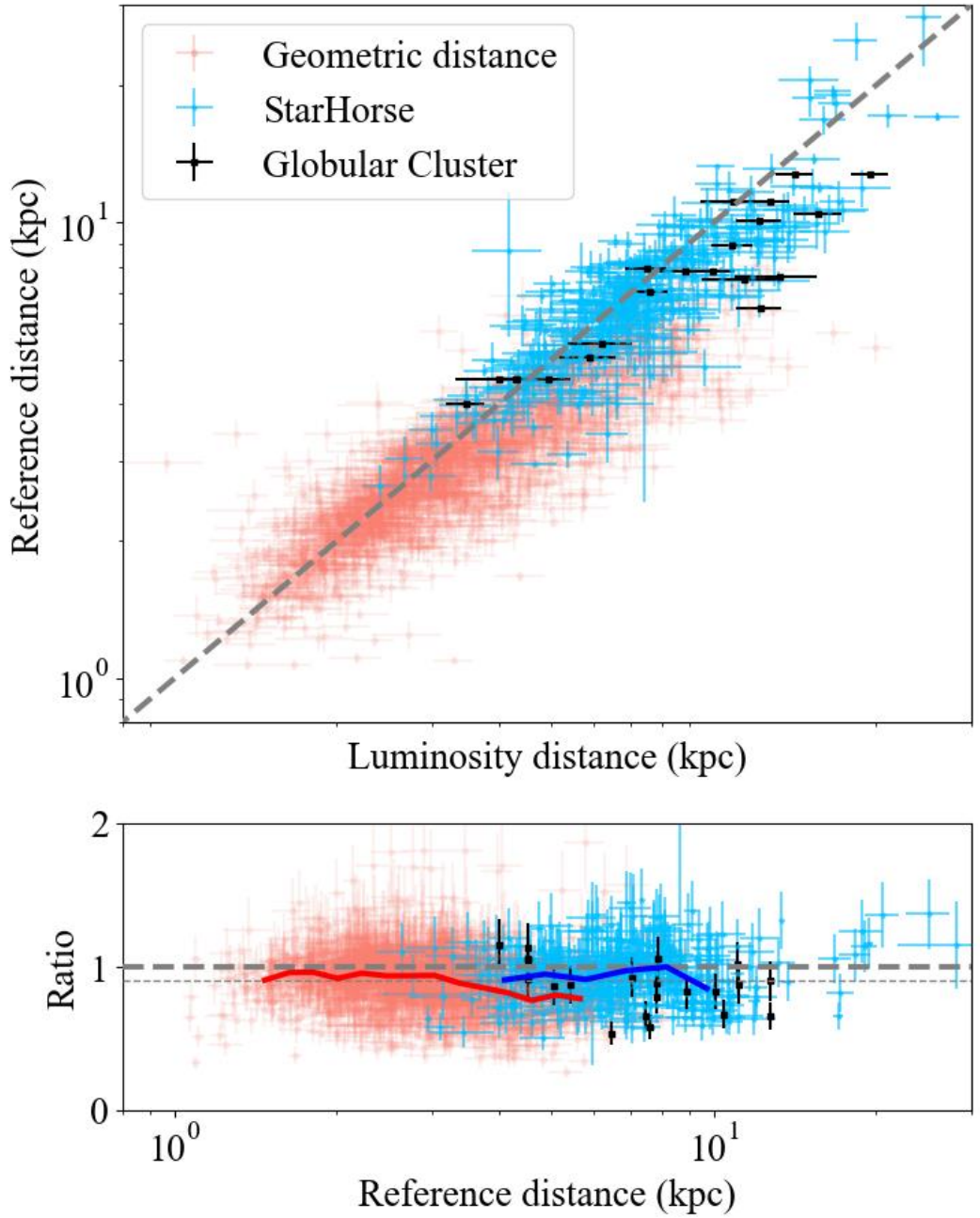

Is the line-of-sight velocity bad due to the variability? – NO

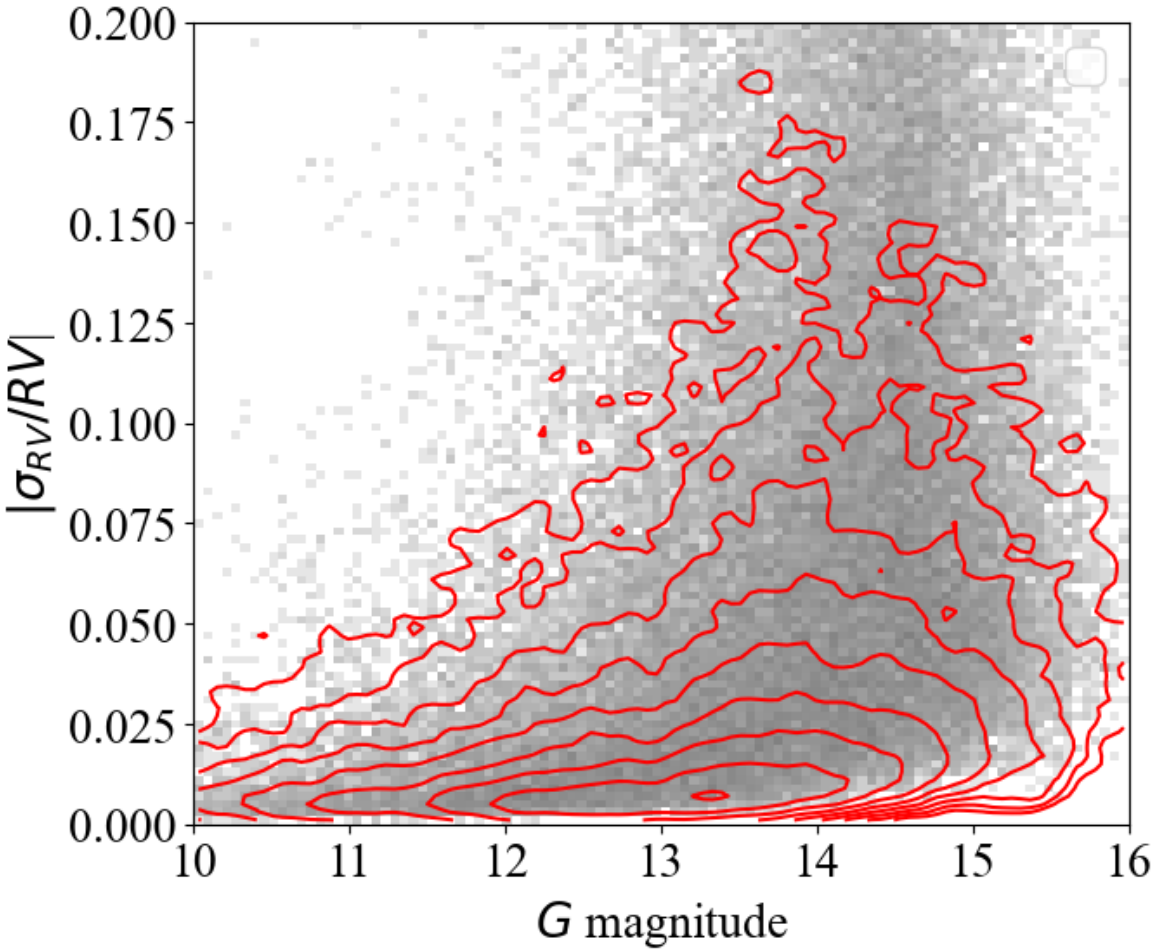

- Black 2D histogram in the background: Randomly selected Gaia DR3 stars
- Red contour in the foreground: LA-LPVs in this sample

The identical distribution in this plane verified the reliability of the Gaia line-of-sight velocity measurement for these LA-LPVs

Kinematics of the LA-LPV sample

Bar signature: Quadrupole v_R pattern

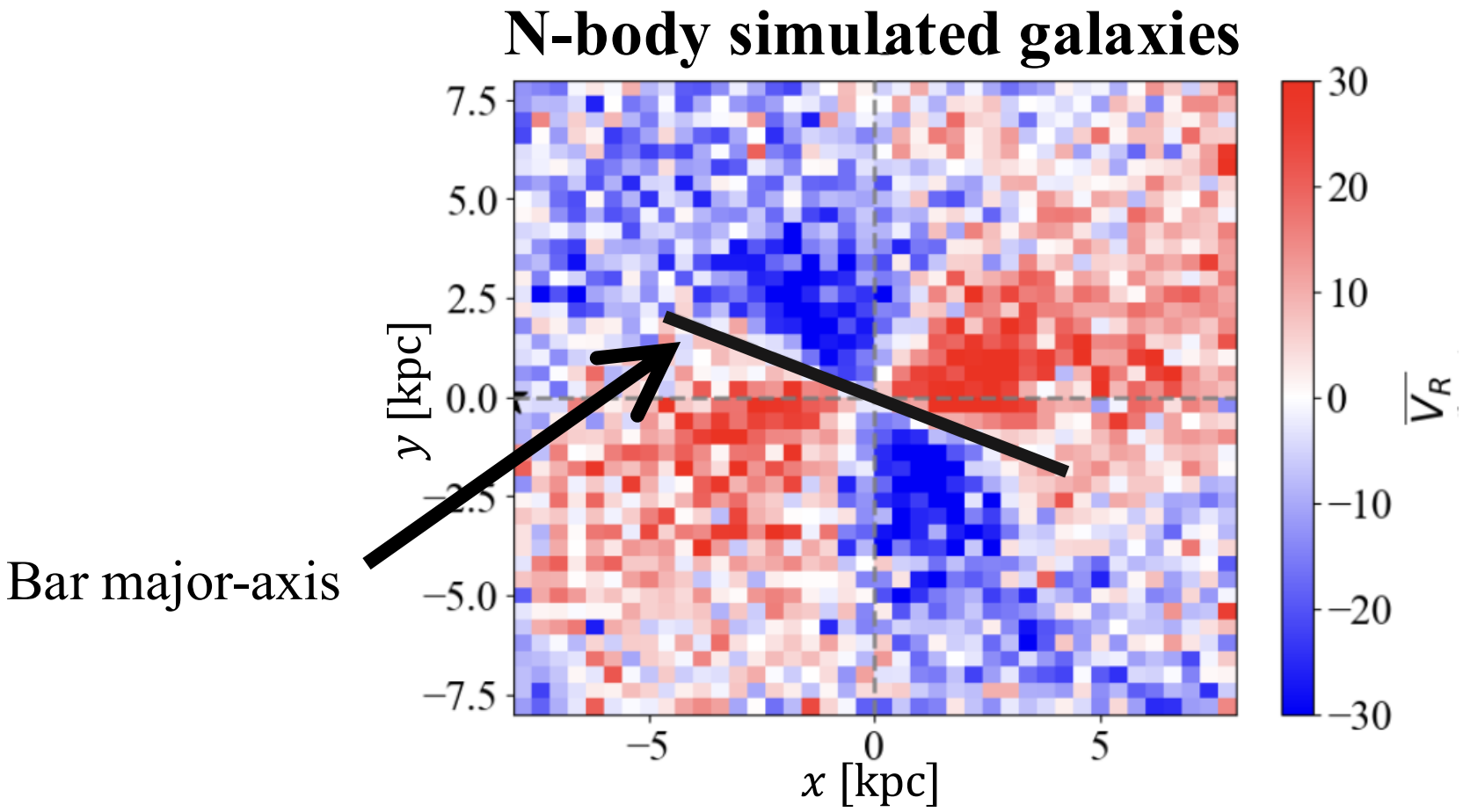

Kinematics of the LA-LPV sample

- No obvious signal is seen, which means the inner Galactic is vertically dynamically quiet

Mean v_z map

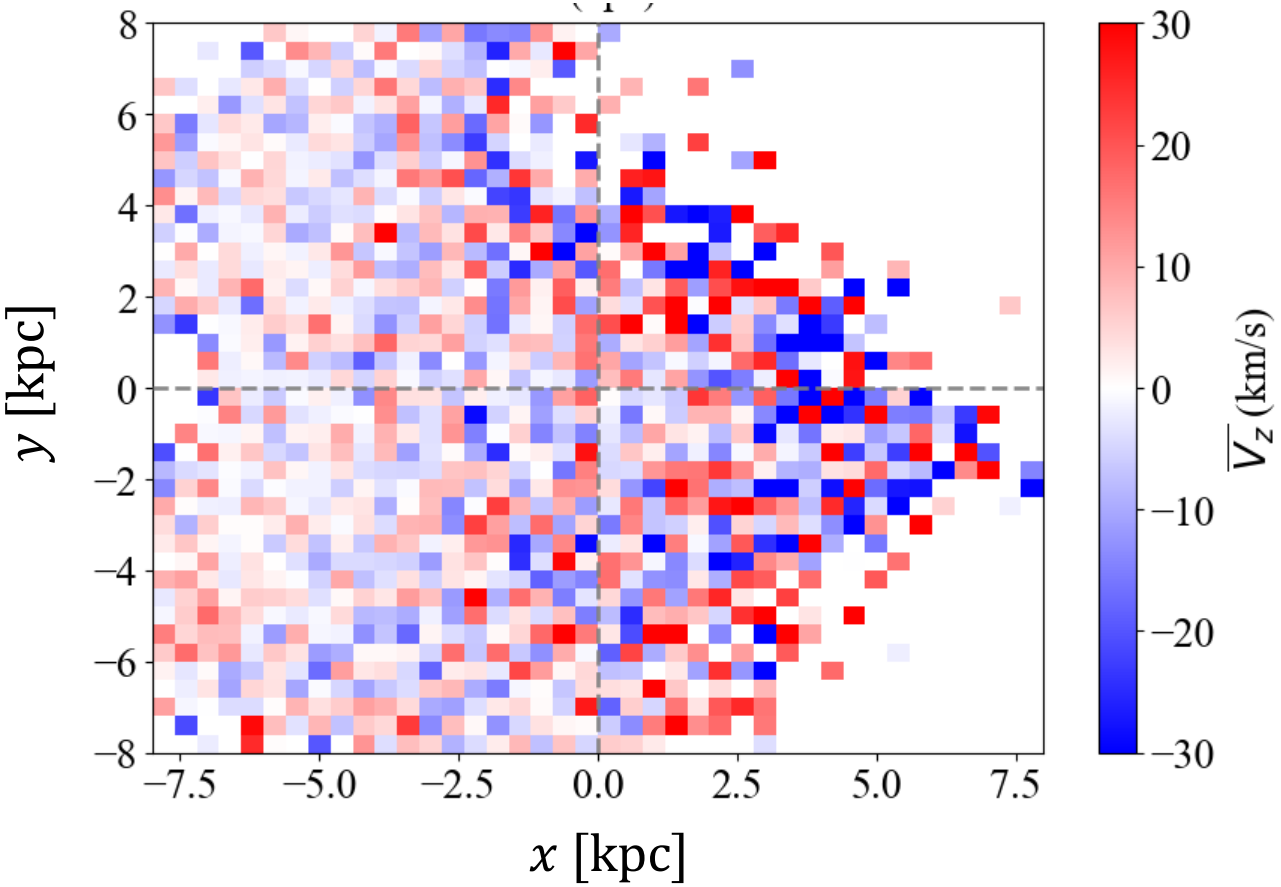

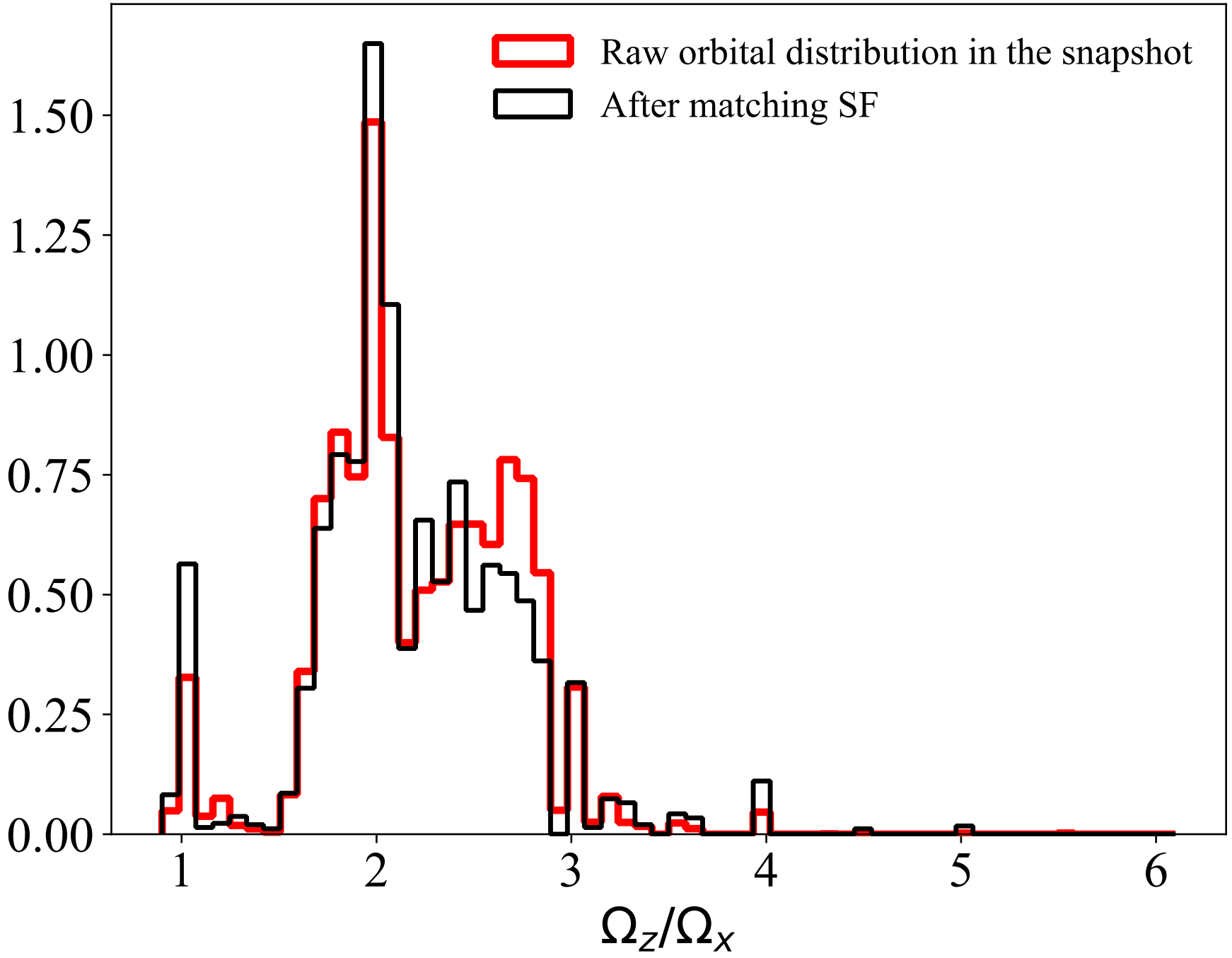
Raw orbital distribution in the snapshot
After matching SF
1.50
1.25
1.00
0.75
0.50
0.25
0.00
1
2
3
4
5
6
Ω_z/Ω_x

Quadrupole pattern in ν_R

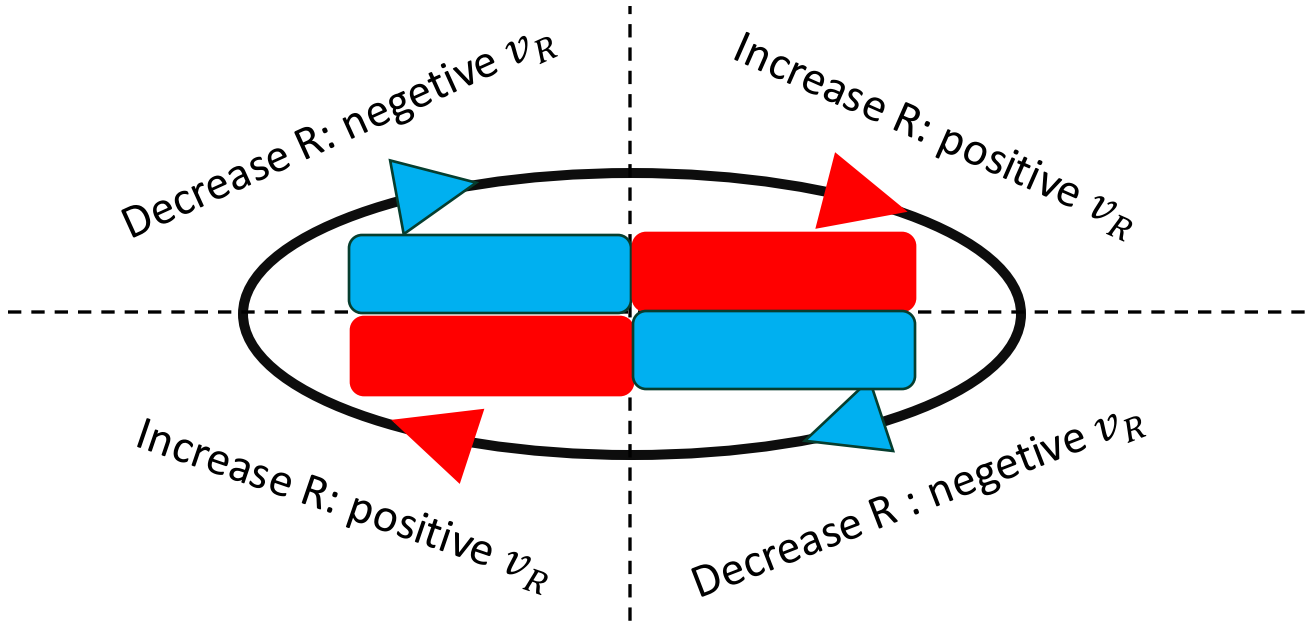

Kinematic signature of the bar:

Quadrupole pattern in v_R

In the rest frame of the bar:

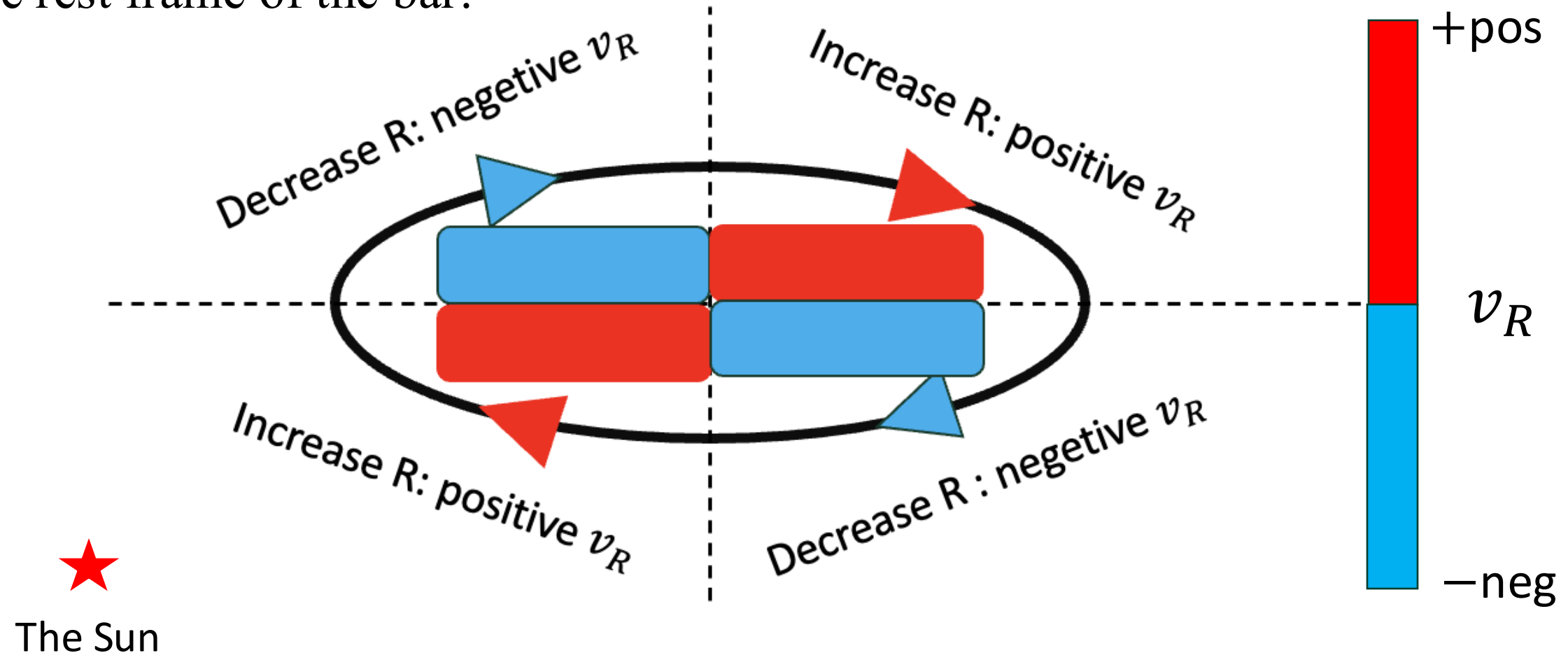

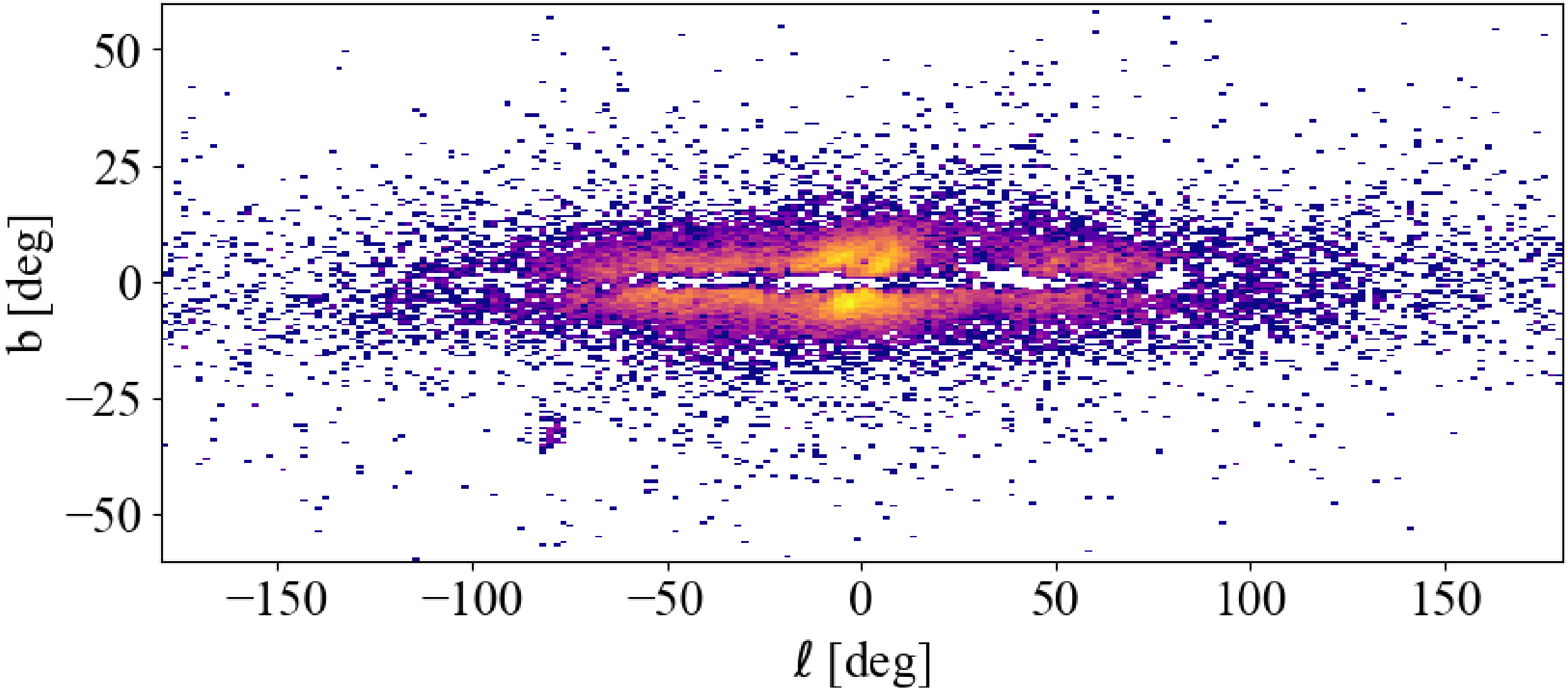
50
25
0
−25
−50
b [deg]
−150
−100
−50
0
50
100
150
ℓ [deg]

Why the spatial selection function is minor

- Gaia full-sky coverage avoid sharp cutoff around the edge of footprints (unlike OGLE and APOGEE)
- Mostly photometric selections avoid stronge selection function in magnitude
- The amplitude and period selections restrict the brightness of the star to $-7 < M_{JK} < -8$, which cancel out the magnitude selection function to the first order

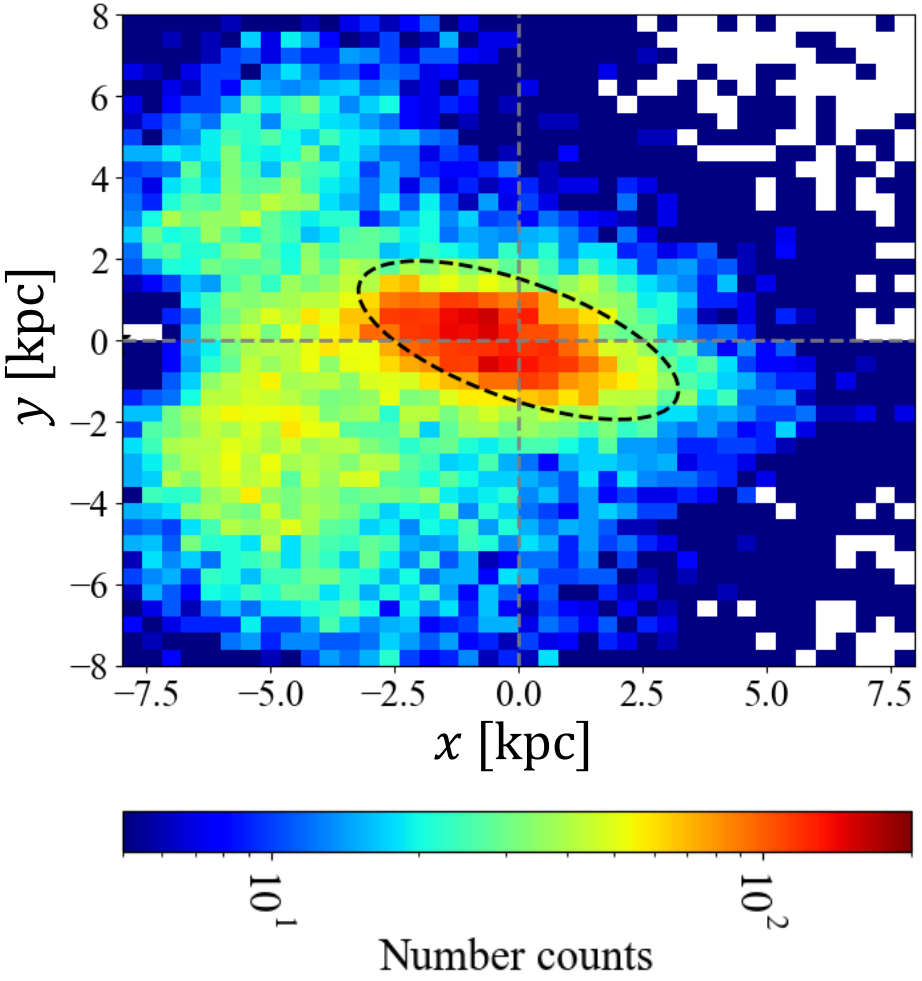

Kinematics of the LA-LPV sample

Sanity check: Mean azimuthal velocity map

- Constant rotation curve at large radii (around the solar vicinity)
- Rotation drops to almost zero at the very inner centre (see Leung+23)

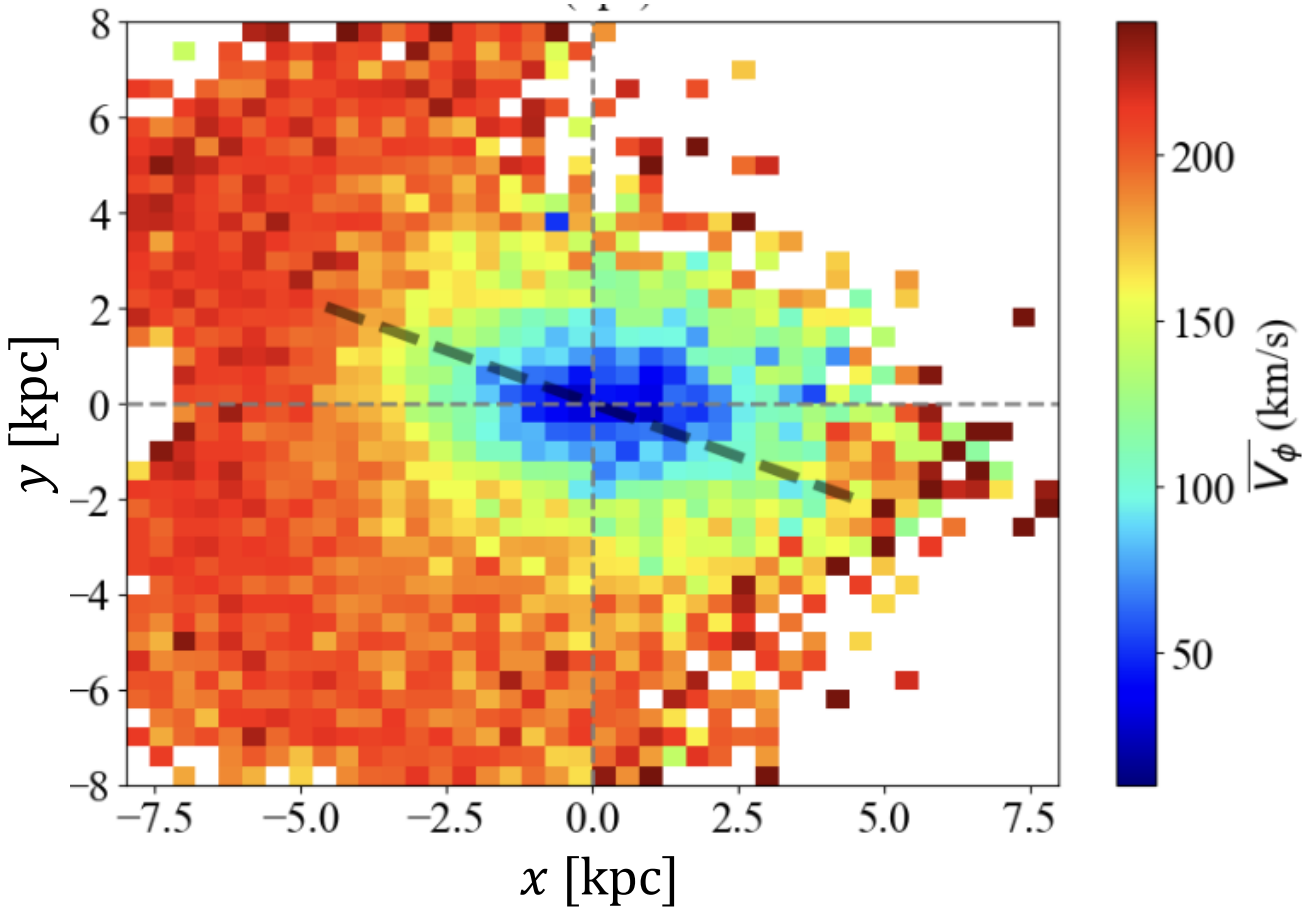

Observed

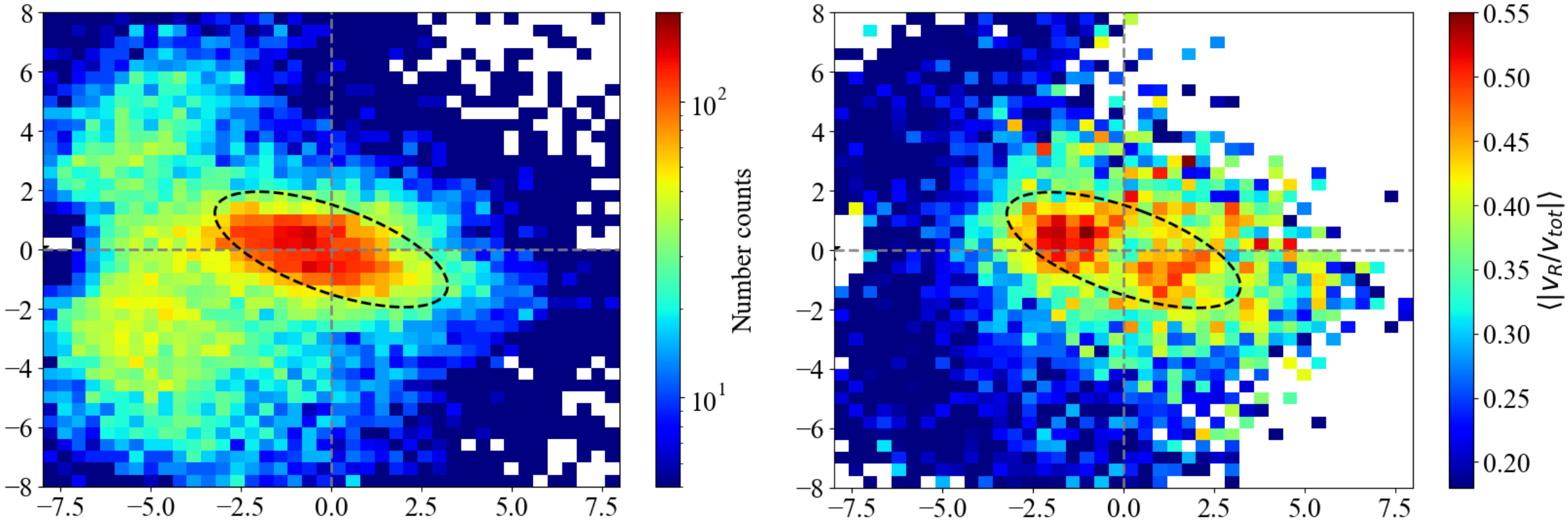
8
6
4
2
0
−2
−4
−6
−8
−7.5
−5.0
−2.5
0.0
2.5
5.0
7.5
10^2
10^1
Number counts
0.55
0.50
0.45
0.40
0.35
0.30
0.25
0.20
$\langle |v_R/v_{tot}| \rangle$

Observed

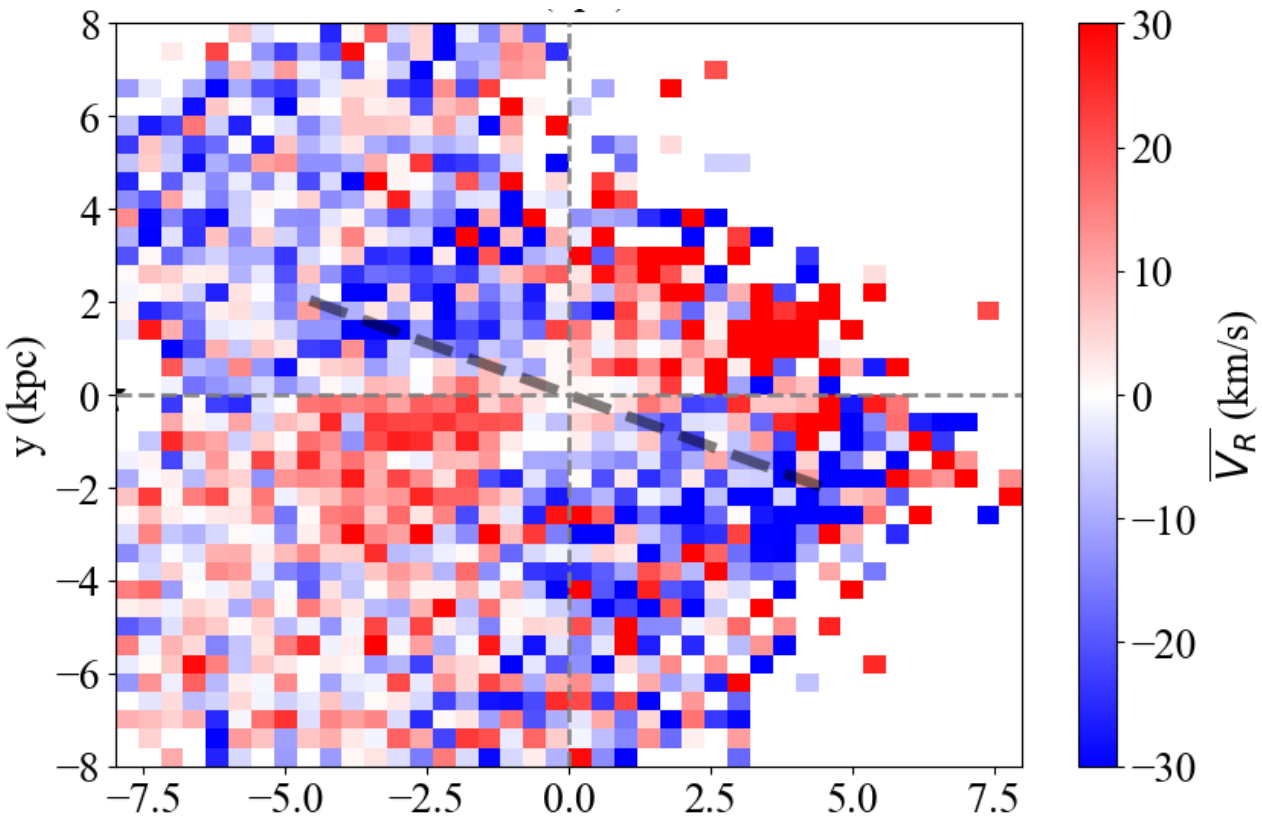
y (kpc)
8
6
4
2
0
−2
−4
−6
−8
−7.5
−5.0
−2.5
0.0
2.5
5.0
7.5
30
20
10
0
−10
−20
−30
$\overline{V_R}$ (km/s)

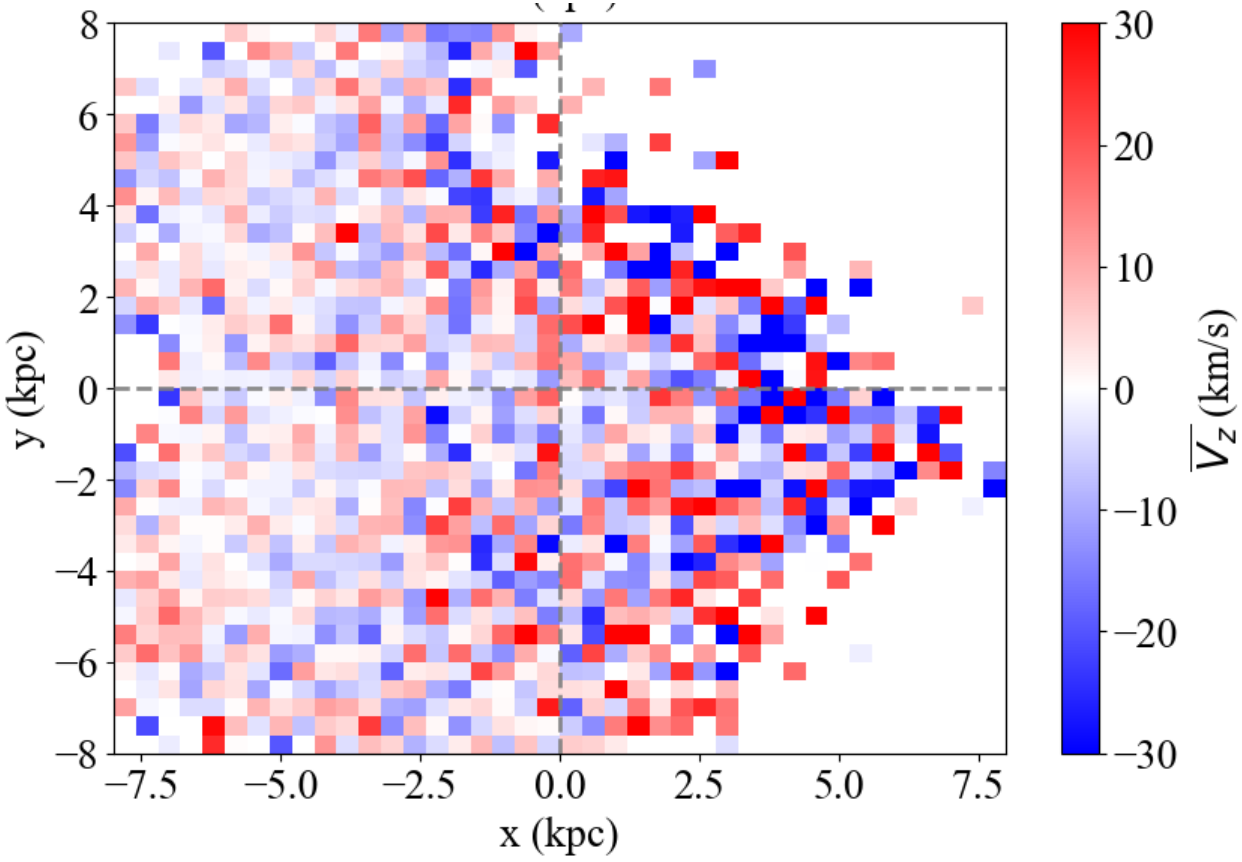
y (kpc)
8
6
4
2
0
−2
−4
−6
−8
−7.5
−5.0
−2.5
0.0
2.5
5.0
7.5
x (kpc)
30
20
10
0
−10
−20
−30
$\overline{V_z}$ (km/s)

Matching the spatial selection function (SF)

- To fairly compare the N-body simulation to the observation, we need to apply both the uncertainty and the selection function.

- For each observed star, we find its closest match in the Cartesian space from the simulated stars, and we discard the rest of simulated stars that are failed to become a closest-match

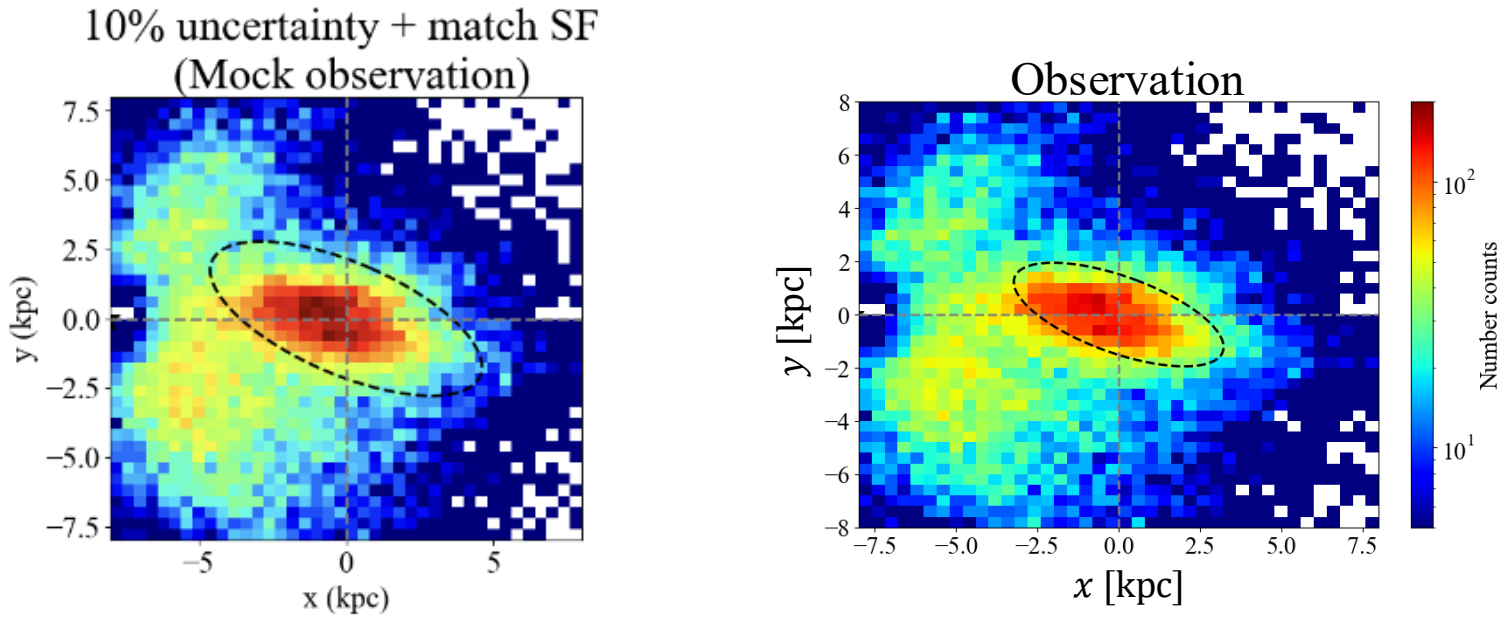

Matching the spatial selection function

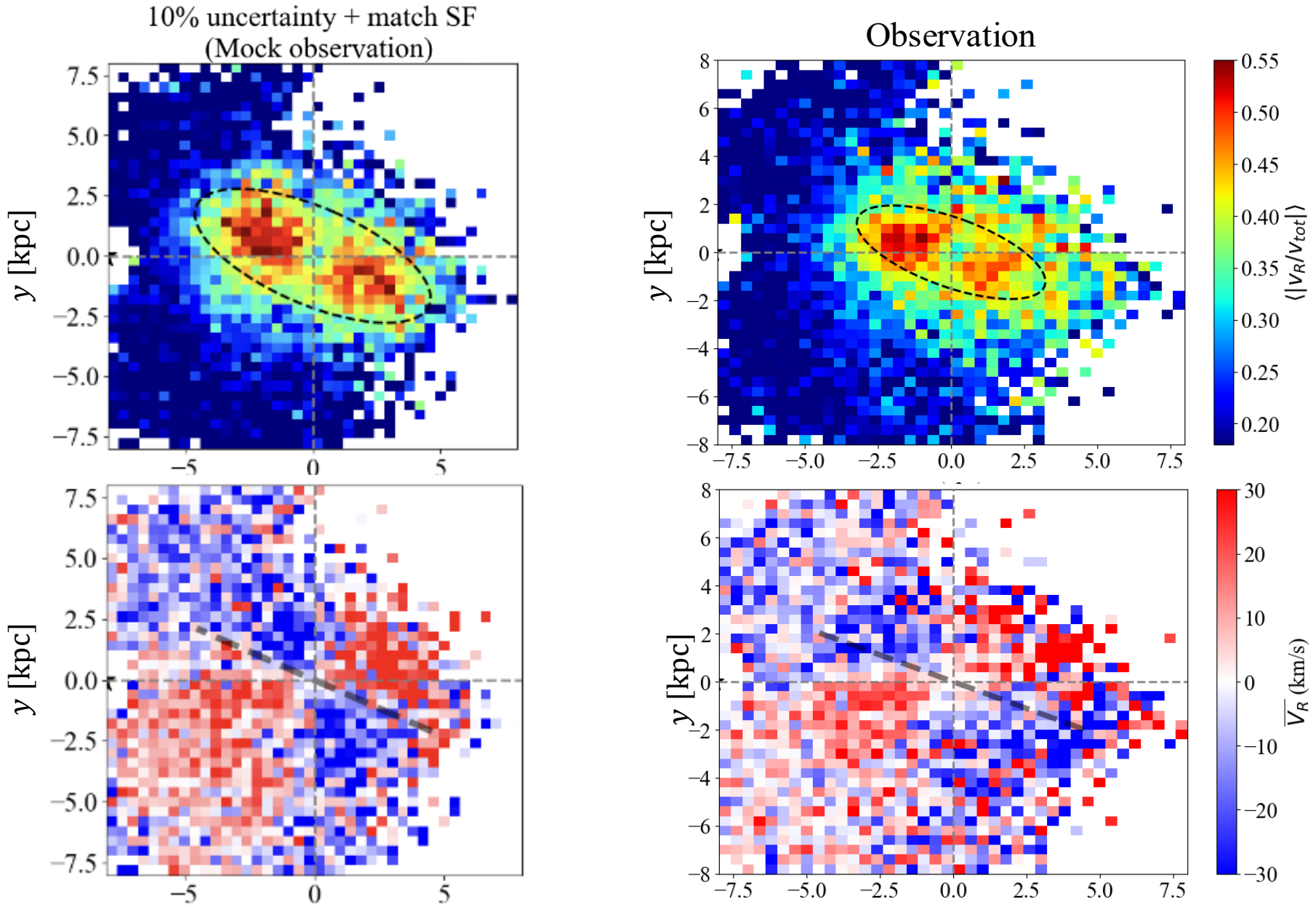

Bar kinematics in the N-body simulation

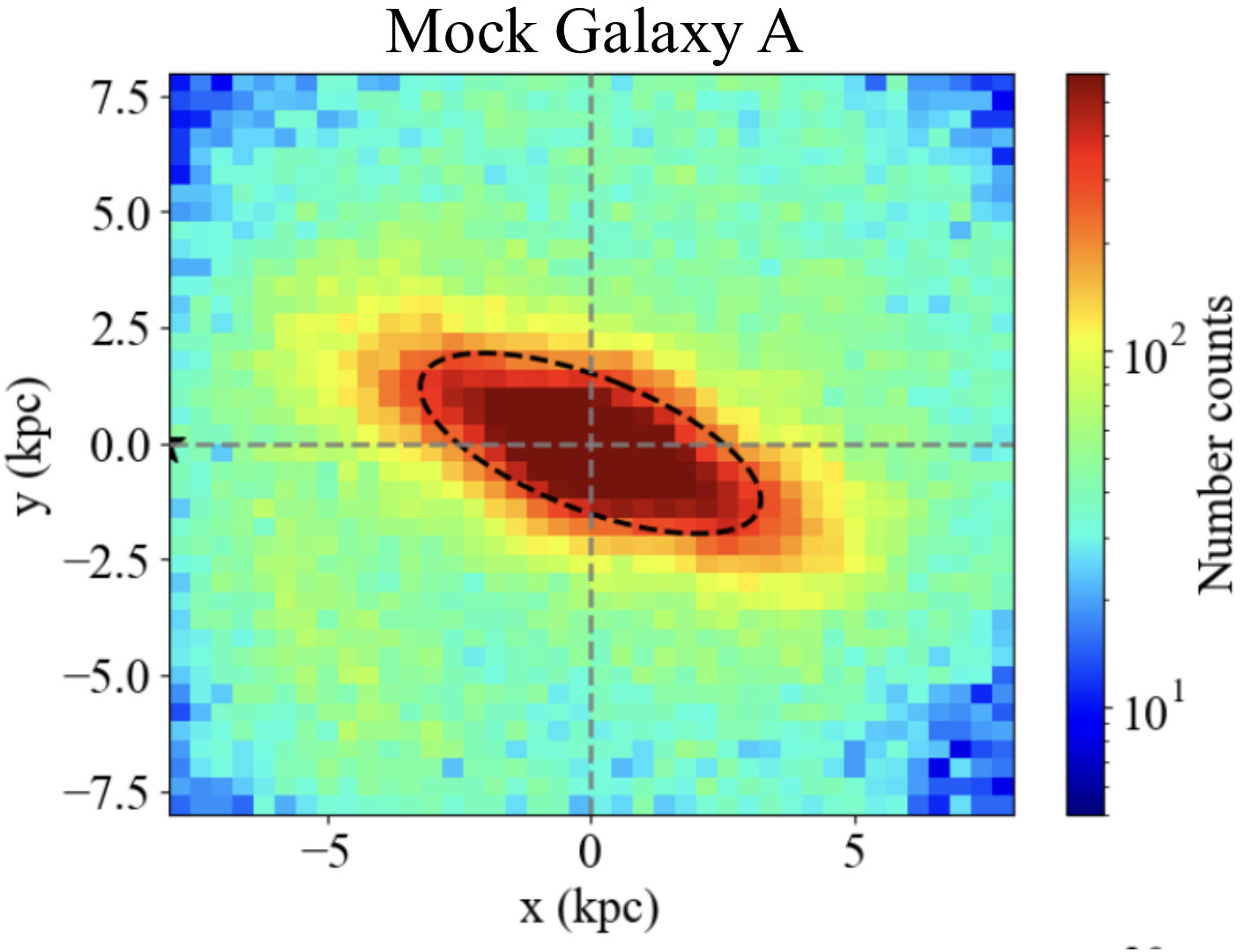

Bar kinematics in the N-body simulation

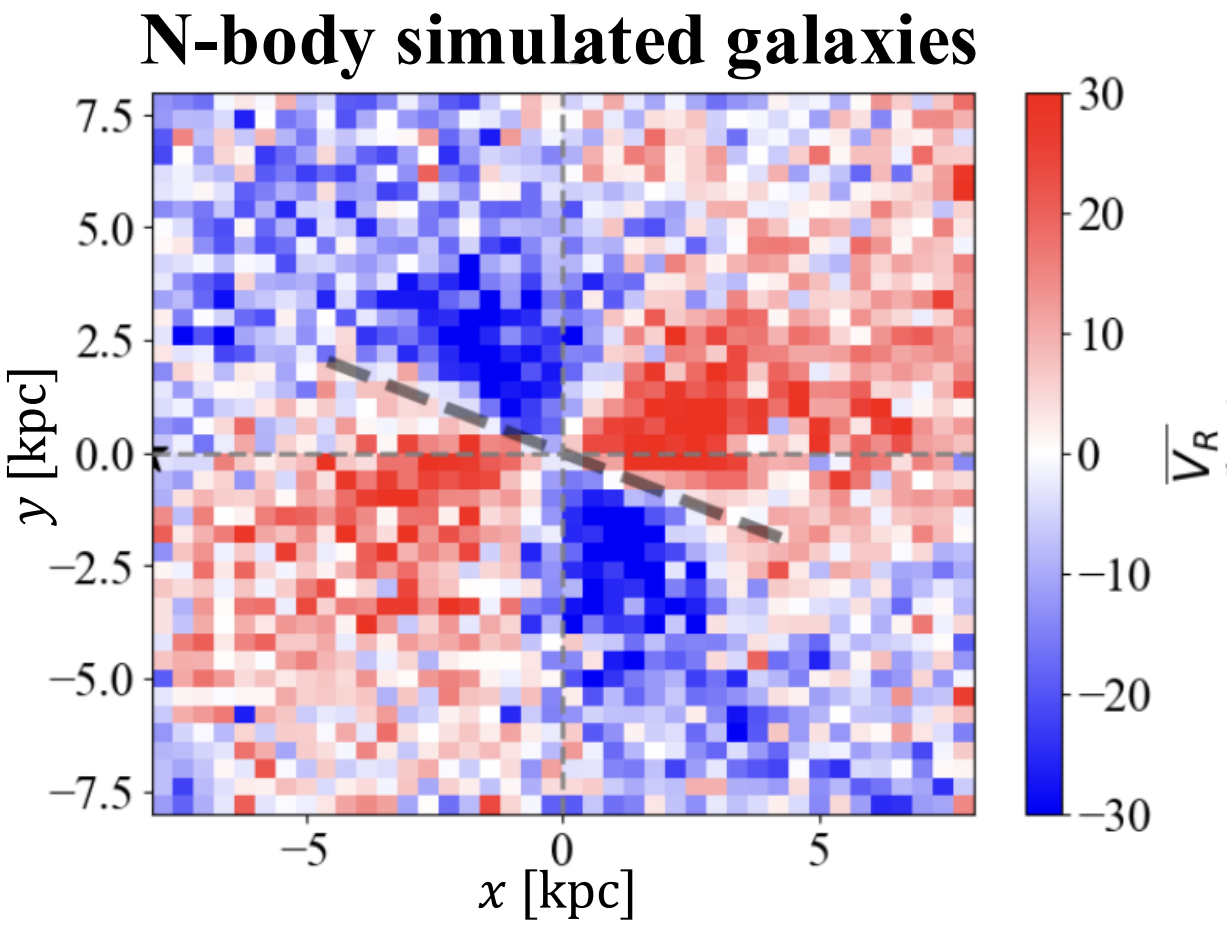

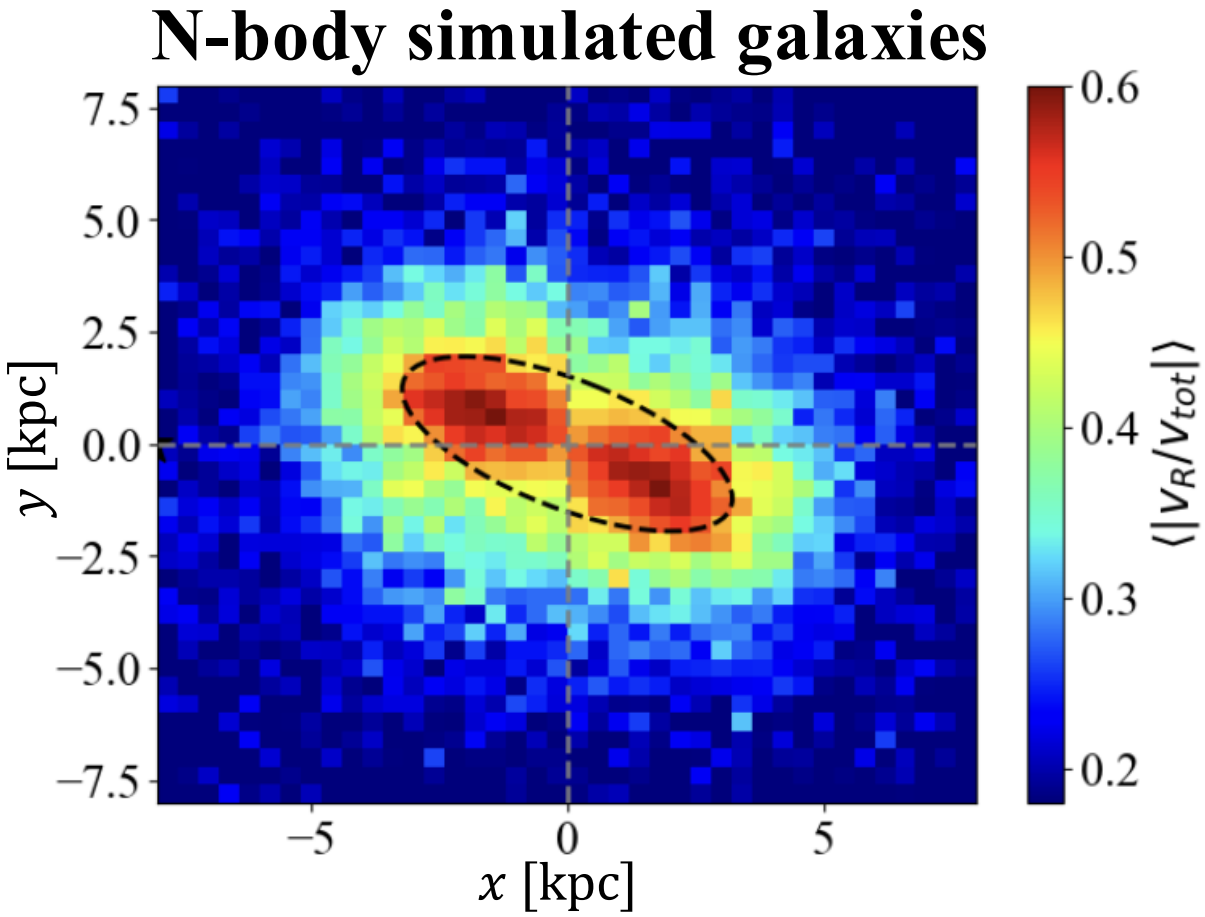

Effects of the heliocentric distance uncertainty

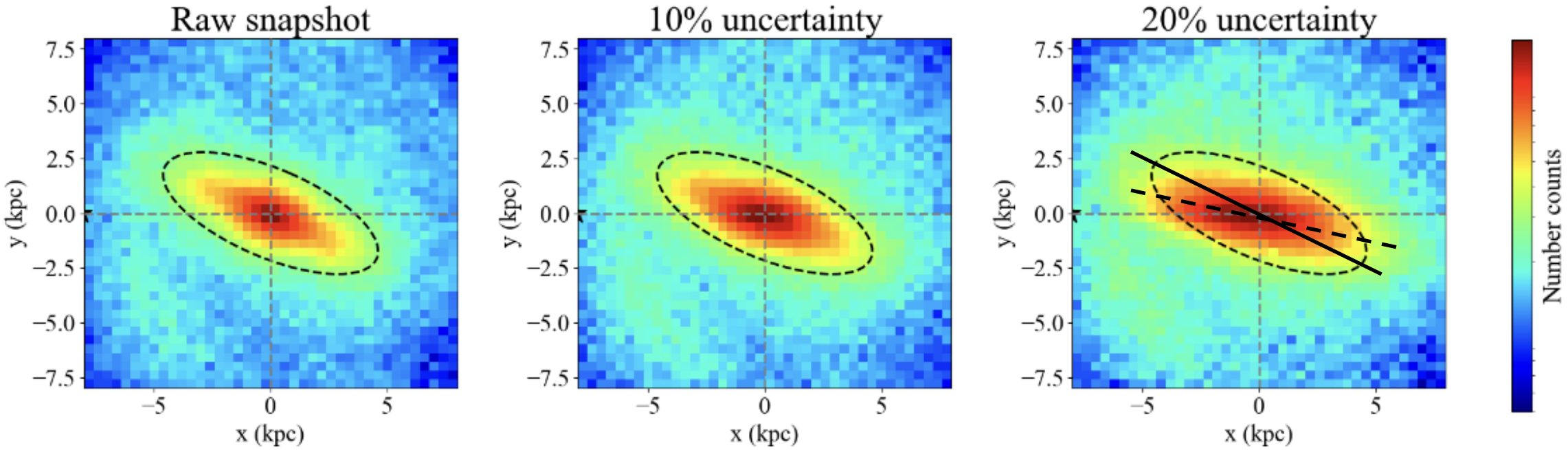

- Distance uncertainty smears each star along the line-of-sight direction bending the major-axis of the bar from its truth to the Sun-GC line

Effects of the heliocentric distance uncertainty

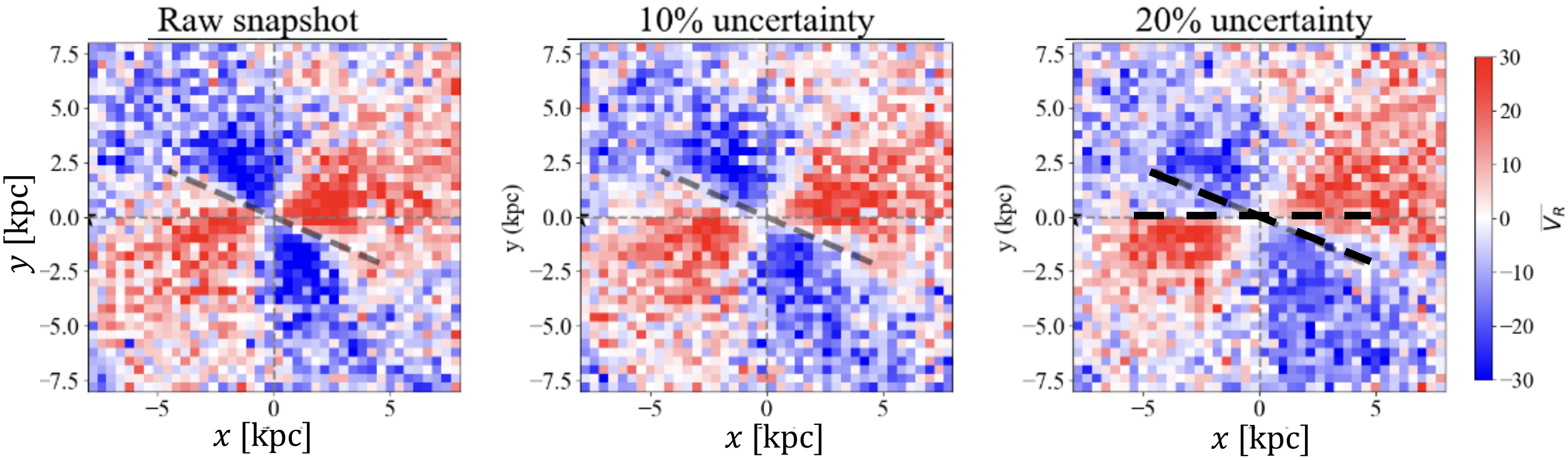

- The $\langle v_R \rangle$ map is even more biased, which demonstrates that the distance uncertainty in the Galactic bar region propagated in a non-Gaussian manner!

Effects of the heliocentric distance uncertainty

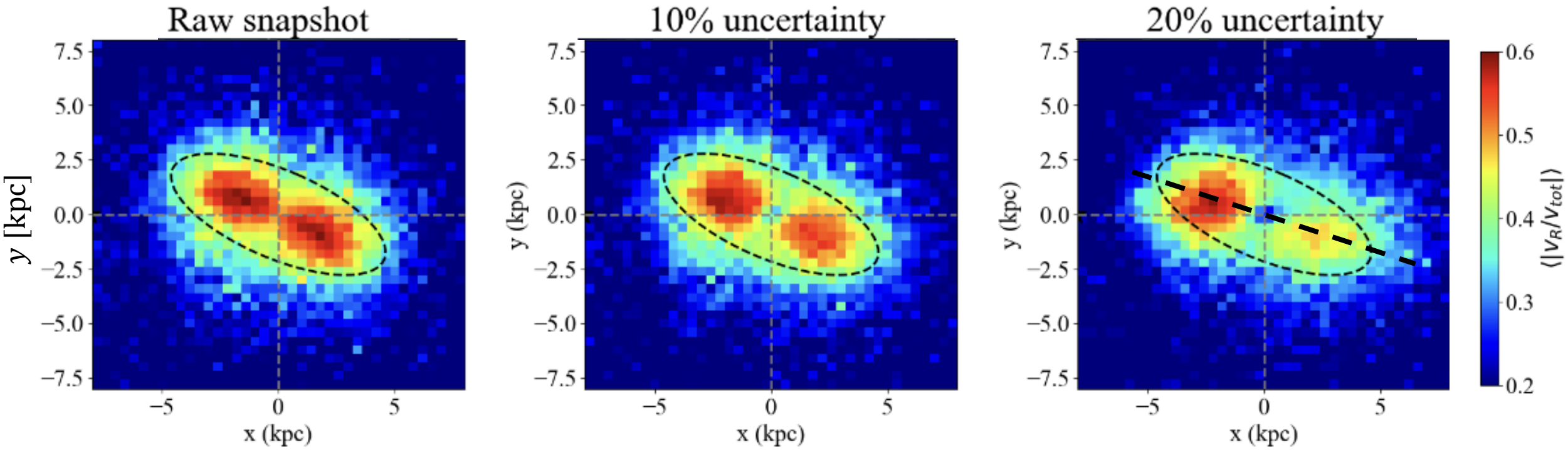

- The $\langle |v_R|/v_{tot} \rangle$ maps are much less affected by the distance uncertainty comparing to the $\langle v_R \rangle$ map because it is dimensionless

Estimation of the pattern speed

- Dehnen+23 developed a method to extract pattern speed from simulations using the continuity equation

$$\partial\rho/\partial t + \nabla\cdot(\rho\bar{\boldsymbol{v}}) = 0 \longrightarrow \Omega = \frac{\int \mathrm{d}^3\boldsymbol{x}\,\rho\left[W\bar{\dot{\varphi}} + \frac{\mathrm{i}}{m}\bar{v}_R(\partial W/\partial R)\right]\mathrm{e}^{-\mathrm{i}m\varphi}}{\int \mathrm{d}^3\boldsymbol{x}\,\rho\,W\,\mathrm{e}^{-\mathrm{i}m\varphi}}.$$

- Can't directly apply to any observation because:
  - The continuity equation can't handle uncertainties
  - This formulation also can't accept the azimuthal selection function

- We can test how much these two observational caveats would influence the pattern speed calculation using the N-body simulation snapshots

In-plane distribution of bar stars

- Stars with greater Ω_Z/Ω_X value span **larger** radius and reside **farther** from the Galactic centre

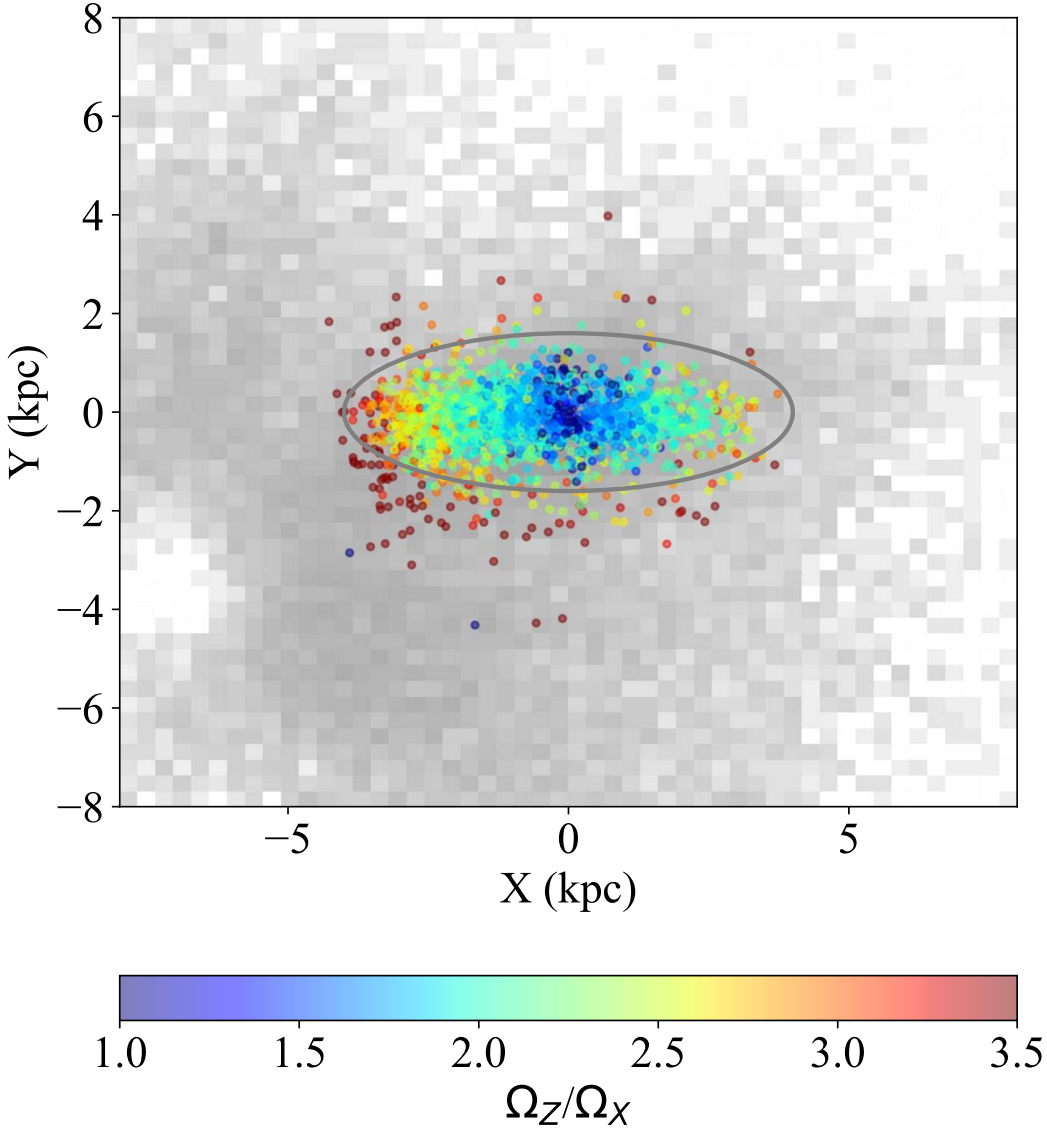

Bias due to the distance uncertainty

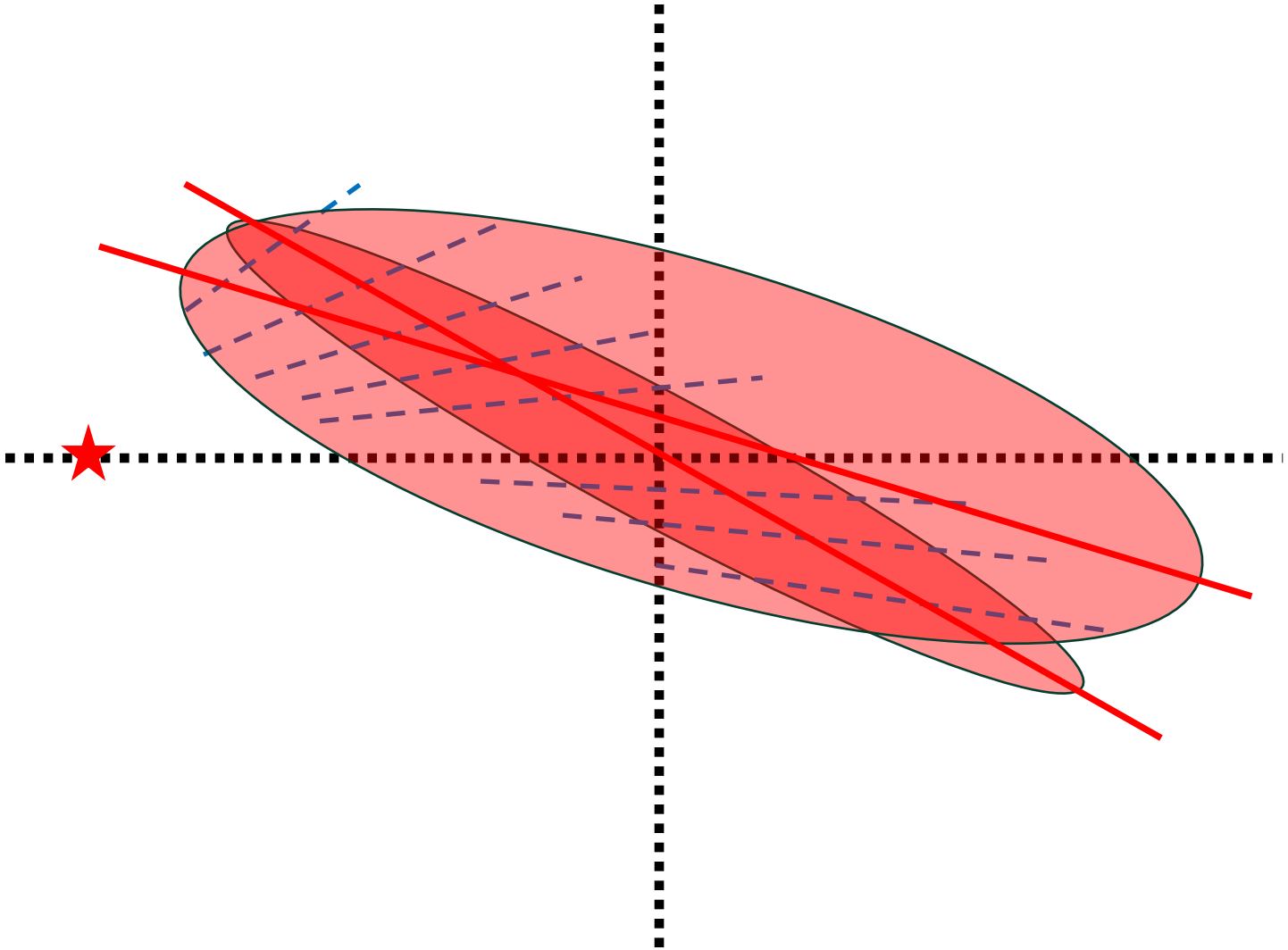

Dehnen+23's Fourier method

$$\partial\rho/\partial t + \boldsymbol{\nabla}\cdot(\rho\bar{\boldsymbol{v}}) = 0 \longrightarrow \Omega\frac{\partial\rho}{\partial\varphi} = \boldsymbol{\nabla}\cdot(\rho\bar{\boldsymbol{v}}),$$

$$\Omega = \frac{\int \mathrm{d}^3\boldsymbol{x}\,\rho\left[W\bar{\dot{\varphi}} + \frac{\mathrm{i}}{m}\bar{v}_R(\partial W/\partial R)\right]\mathrm{e}^{-\mathrm{i}m\varphi}}{\int \mathrm{d}^3\boldsymbol{x}\,\rho\,W\,\mathrm{e}^{-\mathrm{i}m\varphi}}. \longleftarrow \Omega\int \mathrm{d}^3\boldsymbol{x}\,\rho\,\frac{\partial w}{\partial\varphi} = \int \mathrm{d}^3\boldsymbol{x}\,\rho\bar{\boldsymbol{v}}\cdot\boldsymbol{\nabla}w,$$

$$\Omega + \frac{\mathrm{i}}{m}\frac{\dot{\Sigma}_m}{\Sigma_m} = \frac{\sum_i \mu_i\left[\dot{\varphi}_i W_i + \frac{\mathrm{i}}{m}\dot{R}_i(\partial W/\partial R)_i\right]\mathrm{e}^{-\mathrm{i}m\varphi_i}}{\sum_i \mu_i W_i\,\mathrm{e}^{-\mathrm{i}m\varphi_i}}$$

where $W(R) = (1-Q)^2(1+2Q)$ with $Q = \dfrac{R^2 - R_\mathrm{m}^2}{R_\mathrm{e}^2 - R_\mathrm{m}^2}$,

$$\ln L(\overline{V_i}, \sigma_i^{\star}) = -\frac{1}{2} \sum_{j}^{N} \left[\ln(\sigma_i^{\star 2} + \sigma_{i,j}^2) + \frac{(v_{i,j} - \overline{V_i})^2}{\sigma_i^{\star 2} + \sigma_{i,j}^2} \right], \qquad (3)$$